Development of Floating Rubber-Concrete Isolation Slab System for 3D Vibrations

Nahal Kamil Fayyadh[1], Farzad Hejazi[2]*, and Thomas Chong[3]
[1] Postgraduate Researcher, Department of Civil Engineering, University Putra Malaysia, Malaysia
[2] Senior Visiting Academic, Department of Civil and Structural Engineering, University of Sheffield, UK
[3]- Hercules Structures System LTD, London, United Kingdom
*Email of Corresponding Author: Farzad@fhejazi.com

Abstract: Nowadays by implementing of various machineries and equipment, the structures are subjected to multidirectional vibrations as combination of vertical and horizontal cyclic oscillations. The slabs are the main structural components, imposed to the dynamic loads due to vibrating generator machines and the load is transferring from slabs to the foundation through the girders and columns.

Recently, application of the high damping rubber bearings to the structures as base isolator systems to dissipate imposed dynamic loads is frequently considered by design engineers, mainly for controlling horizontal vibrations. However, in order to isolate machine-induced vibrations, it is required to isolate the machine itself within the story.

Therefore, in the present research an attempt has been made to develop a floating rubber-concrete isolation slab system (FRCISS) by implementing High Damping Rubber (HDR) under the floating slab system. The components of the proposed system are designed based on required criteria and the performance of the developed FRCISS in reducing vibrations in both horizontal and vertical directions are investigated through finite element method.

Thereafter, two prototypes of FRCISS slabs have been casted and experimentally tested under horizontal and vertical cyclic loadings by using dynamic actuator in order to validate the model. Eventually, the new proposed FRCISS is applied on lab-size 3-story, 1-bay buildings numerically. In each building, the floating system is installed within a different story and is subjected to dynamic load. Then the dynamic response of the structures with floating systems are compared with the dynamic response of conventional structures in order to assess the capability of FRCISS to diminish vibration effect.

For interior vibrations, the lateral drifts in the structure with floating systems in the 1st, 2nd, and 3rd stories under horizontal cyclic loading were reduced by an average 87.33%, 62.21% and 47.08%, compared to lateral drifts in conventional structures, respectively, while the deflection under vertical loading was reduced by 11.1%. Whereas, the average drift reduction values were 69.68%, 26.08%, and 20.18% under the north-south seismic component, and 74.03%, 17.1%, and 16.55% under the east-west seismic component, for the modified buildings compared to conventional buildings. The current study contribution is summed up in demonstrating the possibility of implementing HDR in the floating slabs to isolate horizontal and vertical vibrations and protect the machinery.

Keywords: High Damping Rubber, Horizontal and Vertical Vibration Isolation, Machinery Vibration, Floating Slab System, Displacement-Controlled Cyclic Loading.

1. Introduction

Reinforced Concrete structures are often vulnerable to vibrations in all directions, mainly in the horizontal and orthogonal plane directions, generated at the ground level by earthquakes or at higher levels by wind loads. In contrast, little attention has been drawn to vertical vibrations (Button *et al*. 2002) since most of the structures are designed to carry gravity loads and less focused on potential of failure under vertical vibrations (Papazoglou and Elnashai 1997).

Seismic loadings are mostly investigated for its horizontal component causing damage to buildings due to the lateral displacements and story drifts. However, some earthquakes, show that vertical component contributes a destructive energy and even exceeds horizontal component effects (Al-Rifaie *et al*. 2015). The effect of vibrations in the horizontal direction is seen mostly in the joints, specifically slab-column or slab-wall connections (Rha *et al*. 2014) which can cause serious deterioration in the structural membranes due to lack of flexibility in the connection regions. Almeida *et al*. (2016) found out that horizontal vibrations, represented by cyclic loadings can cause damage to the slab and column which leads to low drift and energy dissipation. Whereas, number of efforts have been made on studying the dynamic response of slabs under vertical vibrations. Foglar and Göringe (2015) have found that deflection in prestressed concrete slabs can increase in higher rates under cyclic vertical loading compared to static vertical loading.

One of the most common measures to deal with horizontal vibrations in multistory buildings is the use of high damping rubber (HDR) bearings in base isolation. It was shown by Hu and Zhou (2020), that the HDR bearings in a base isolation are able to reduce lateral displacements of the superstructure under extreme earthquake excitations. In buildings constructed near metros, Pan *et al.* (2018) have found that the base isolation with thick HDR bearings controls metro generated vibrations more efficiently than thin HDR bearings. Additionally, shear stresses in HDR bearings are highly affected by the compressive (vertical) loads applied on the bearings. However, the latter have no influence on the bearing equilibrium response (Wei *et al.*, 2019).

Woon and Hejazi (2019) have shown that high damping rubber can be used in joints of precast structures to dissipate energy under lateral cyclic loadings. They also have revealed that HDR is capable of dissipating energy under vertical cyclic loading. Moreover, In a study conducted by Warn and Whittaker (2008), the performance of low-damping rubber system in bridges under vertical excitations of earthquakes has been investigated and results showed an amplification in the vertical response to earthquakes. In addition, high damping rubber could function as a tuned mass damper (TM-HDR) and reduce vibrations in taut cables (Cu *et al*. 2017).

While damping rubber has been implemented almost exclusively in horizontal vibration control, a different approach has been used for controlling vertical vibrations generated mainly in railways by vehicles or in building by vibrating machines which is the use of floating slab/ floating floor systems. It comprises a floating slab over the main structural slab and an interlayer of rubber in between. The use of damping pads under floating slabs can, as well, reduce vibration levels (Liang et al., 2019). Moreover, the combination of two isolation methods: i.e. base-isolation of buildings and floating slab track can enhance the vibration level reduction (He et al. 2020). This technique of a floating slab isolated from the layer beneath is also utilized in multistory buildings where the floor inside a story is isolated from the rest of the building. This partial mass isolation in multistory buildings has been investigated by many authors. Anajafi and Medina (2018) have shown in their research work that a partial isolation of 5% and 90% of the mass, simulates the function of TMD and base-isolation in controlling inter-story drifts.

The floating slab is cast separately from the structural slab and the resilient layer works as an isolation layer in between. The main purpose of the intermediate layer is to reduce air-borne or structure-borne vibrations induced by either light weight or high weight vibration sources (Kim *et al*. 2018). The resilient layer is well capable of minimizing the vibrations, but their application is restricted to acoustic purposes. Floor isolation technique has also shown a great reduction of seismic demand in prefabricated modular mass timber (MT) constructions (Chen et al. 2020). Increasing the mass-isolation ratio and the flexibility of the laminated visco-elastic materials (LVEM) isolators for floor isolation in a single-story structure can also decrease the seismic

demand (Xiang et al., 2019) and the inter-story drifts (Xiang and Koetaka 2019). Furthermore, floor isolation systems FISs are capable of decoupling accelerations, and reducing structure displacements and inter-story drifts (Casagrande *et al*. 2019).

On the other hand, the high speed engines and machines, when installed on foundations and supports, cause excessive amplitudes vibrations which damage the foundation on which the machines are installed. Machinery-induced vibrations in an inter-story floor with non-isolated machines, are transmittable and cause severe deterioration to the structural membranes (Bergamo *et al*. 2020). Thus, these vibrations should be eliminated and dissipated using some types of isolation passive devices (Mukherjee 2017). The method of isolating residual vibration of ultra-precision machines via passively isolated system showed the altering of the passive device is effective in reducing vibrations and is more economic compared to increasing the base mass or using active isolators (Okwudire and Lee 2013).

Isolation of a whole building can be highly expensive and in order to protect the structure from a specific vibrating source that might induce vibrations to the structural element beneath (such as slab panel) in both vertical and lateral direction, a modified approach of isolation should be used (Ahmadi *et al*. 2004). Regardless to the previous findings, Castellano *et al*. (2015) conducted 3D tests of displacement time-histories in two horizontal axes and vertical load time-history on huge high damping rubber bearings (HDRB). They found that even after failure, the isolators are still capable to endure the horizontal displacement and the vertical load. In another study by Quaglini *et al*., (2016) on five specimens of HDRBs of different types (soft, medium and hard). Assessing the HDRBs was made experimentally under combined vertical compression and cyclic lateral shear. It has been noted that when axial compression increased, it resulted in rising of both shear modulus and damping which makes it important to consider the compression effect when designing the rubber bearings.

By considering the discussed issues related to the conventional isolation systems for lateral and vertical vibrations, there's a need to implement an effective system to minimize the number of required systems for isolation to a single system. This system should have the potential to dissipate energy and diminish vibrations in all three dimensions as well as the capability to be installed in existing constructions.

Therefore, in the present research study, a floating rubber-concrete isolation slab system (FRCISS) is developed by implementing high damping rubber (HDR) as the isolation material. The proposed FRCISS is comprised of an upper slab which is the floating slab, a lower slab that is the main structural slab and an intermediate layer of isolation rubber pads. The initial design is of proposed system is developed and numerically simulated and analyzed under horizontal and vertical cyclic loadings via finite element method and verified through manufacturing and experimentally testing of the prototypes. Then, the proposed FRCISS is applied on a lab-size 3-story, 1-bay building and compared the response with a control structure to evaluate performance of proposed system to diminish effect of vibration.

2. Development of Floating Rubber-Concrete Isolation Slab System

2.1. Development of the Rubber-Floating Slab System

The present research study introduces a potential solution for controlling vibrations in horizontal and vertical directions to avoid of implementing extra features. The proposed FRCISS is developed based on the floating system concept. This system comprises a floating slab in the upper layer, the main structural slab in the lower layer and a high damping rubber bearings as isolators in the interlayer as demonstrated in the Fig. 1.

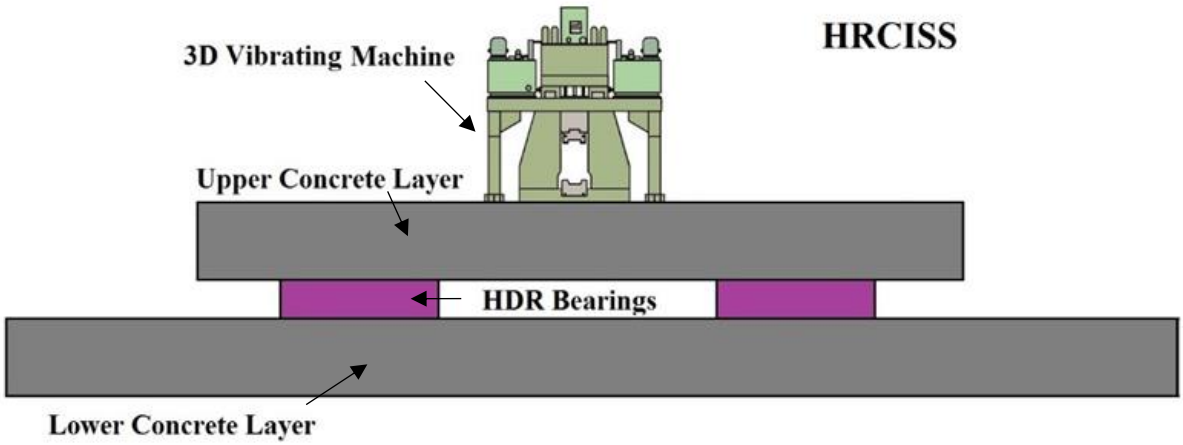

Fig. 1 The proposed floating slab system with HDR bearings

High damping rubber bearings are commonly used in base and mid-story isolation to isolate lateral vibrations generated by earthquakes or wind loadings (Naeim and Kelly, 1999). The presence of the damping rubber in the interlayer of the floating slab system has ability to control vibrations in the vertical direction (Warn and Whittaker, 2008) as well as reducing story drifts and damage in the lateral direction (Gowardhan and Deosarkar, 2015).

A square-sectioned bearing of soft HDR, without steel shims, is used. The selection of square rubber bearings is based on a previous work by Jin *et al*. (2015) which was experimentally conduced on floating floors, under railway vibrations, with different configurations of rubber layer: point-like rubber (square/rectangular), linear rubber and full-surface rubber. The study found that square rubber configuration was better in controlling vertical vibrations.

Whereas, the absence of steel shims will reduce the vertical stiffness in the rubber bearing and hence be suitable to carry low to medium masses. This has been proven via FE by modeling two rubber bearings: HDRB1, with steel shims and HDRB2 without steel shims while both bearings have the same shape factor (Fig. 2). The results shown in Fig. 3 demonstrates the effect that the exclusion of steel layers had on the compressive force and in turn the compressive stiffness of the bearings.

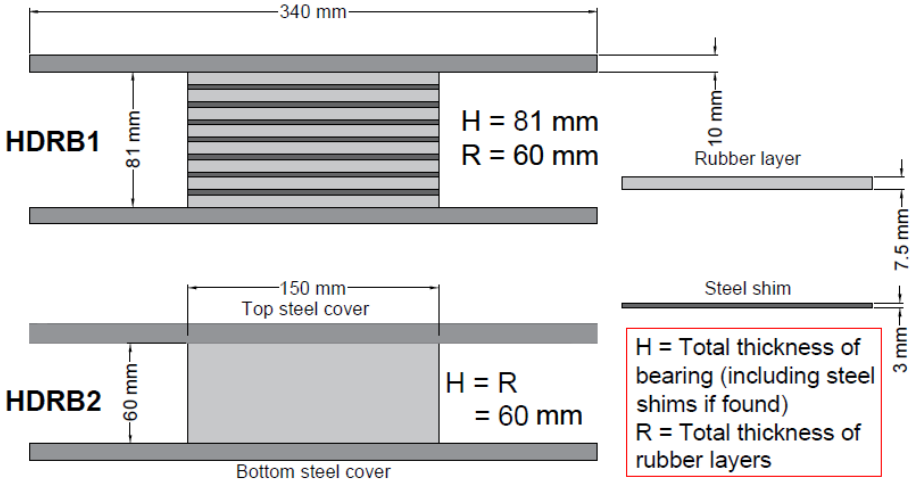

Fig. 2 Configuration of typical and developed HDR bearings for compression testing

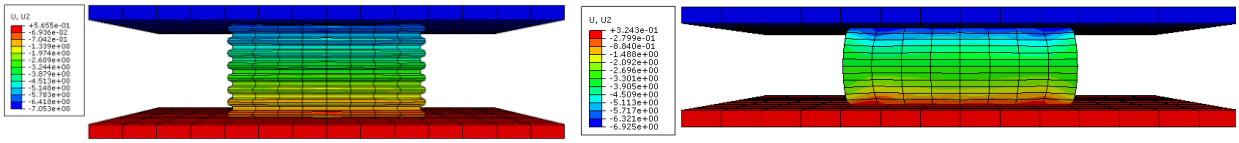

(a) HDRB1 deformation (b) HDRB2 deformation

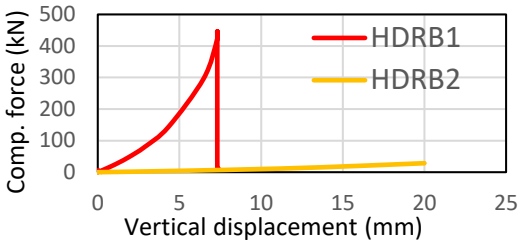

(c) Compressive force-displacement

Fig. 3 Comparison between HDRB1 and HDRB2

The design process of the bearing is based on the load and displacement capacities as well as the floating slab and machine masses. A natural frequency test has been conducted via FEM on the floating slab with and without the isolation layer showed a decrement in the frequency with the presence of rubber bearings, resulting in larger time period and frequency ratio which ultimately led to reduce the force transmissibility of the system.

The equation for the capacity force of the RC slab with accordance to ACI 318-08 (Section 11.11.2.1) is:

$$V_c = \left(2 + \frac{4}{\beta} \right) \lambda \sqrt{fc'}\, b_o d \qquad (2)$$

Where: V_c is the maximum shear force without shear reinforcement, β is the ratio of the long side to the short side for the column cross-section, fc' is the compressive strength, b_o is the perimeter of the support and d is the effective depth of the slab.

Hence, shear force capacity for a 100 mm deep RC slab with 200 mm perimeter is: V_c = 476 KN. Since V_u is less than or equal to 0.5 ØVc, where Ø = 0.75, this means that the factored shear force is equal to: V_u = 143 KN. Hence, the dimensions of the HDR square bearings can be calculated as follows:

Due to the low elevation of the horizontal actuator, the thickness of the rubber bearings is designed as 60 mm. Thus, from equation (2) for a 100% shear strain, the shear stiffness for a single rubber bearing is calculated as: Kh = 0.58 KN/mm. Assuming the shear modulus of the HDR bearing, G to be equal to 0.4 and for 60 mm thickness, the loaded area of the rubber bearing, A will be approximately equal to 150 mm x 150 mm.

The bearing is covered with steel plates and placed between the two slab panels of the modified system in order to control energy and vibration transmission from upper slab layer to the lower slab layer by dissipating the energy and reducing the vibration amplitudes. The relative low stiffness of HDR bearings in the horizontal direction can provide a sufficient decoupling of shear stresses between the two slab layers, while the steel shims in the typical HDR bearing offer high vertical stiffness capable to sustain high vertical loads such in high- and low-rise buildings of large masses (Naeim and Kelly, 1999). However, in this research, the proposed model deals with vibrations induced by low-mass machines.

These sources of vibrations are relatively small in mass and result in very low stresses compared to the overall structural building. Hence, using soft high damping rubber with low shear modulus

and excluding the steel shims can reduce the vertical stiffness in the bearings and in turn may offer a proper isolation for vertical vibrations in addition to the horizontal motion control.

Fig. 4 shows the proposed HDR bearing compared to the typical HDR bearing. Whereas, Fig. 5 demonstrates the expected deformation of the proposed HDR bearing under horizontal and vertical loads, F and P, respectively, where the lateral drift, Δ corresponds to a shear strain, $\gamma = \Delta / H$ and shear stiffness, $K_h = F / \Delta$, and the vertical displacement, δ which leads to a compression strain, $\varepsilon = \delta / H$ and compressive stiffness, $K_v = P / \delta$.

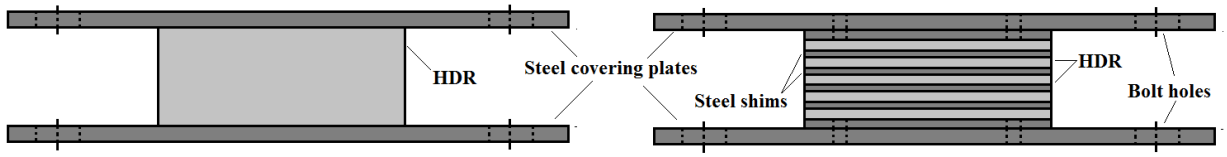

(a) proposed HDR bearing without steel shims (b) typical HDR bearing with steel shims

Fig. 4 Side-view of proposed and typical HDR bearings

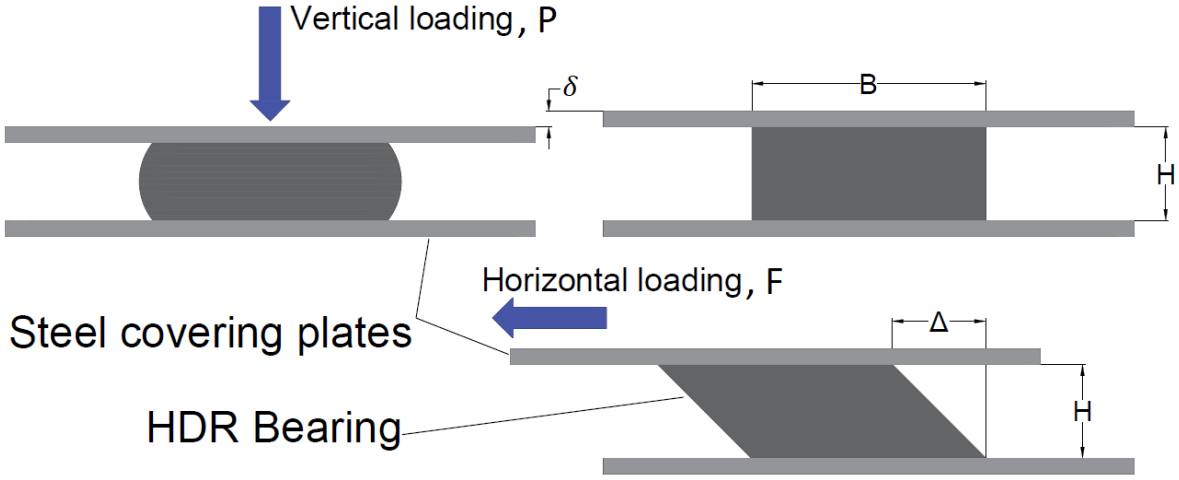

Fig. 5 Deformation of HDR under horizontal and vertical loadings

The relative low stiffness of shim-less HDR in both directions, may allow the upper slab to displace horizontally and vertically under loads below the capacity loads and avoid damage of the slab layer. Fig. 6 displays the installed FRCISS on structural slab with the vibrating machine in a multistory level.

2.2. Identifying the Optimum Position for Bearings

Floating slab is used to mitigate vibrations induced by ground and train motion by using soft isolators located at the corners (Hui and Ng 2009). However, the placement of the isolators at the corners has less desired outcomes since the isolators should be placed under nodal points of the first flexural vibration mode of the floating floor panel in order to optimize the performance of isolators in reducing the critical vibration mode (Hui and Ng 2007). Optimum location of bearings under the floating slab of the present research has been detected by using their technique. It is used for square plates on shaking tables to reduce the critical flexural vibration mode by applying different frequencies. The resulted modes of vibration are analyzed and only the modes with symmetric shapes are considered. The location of isolators should be under the nodal points.

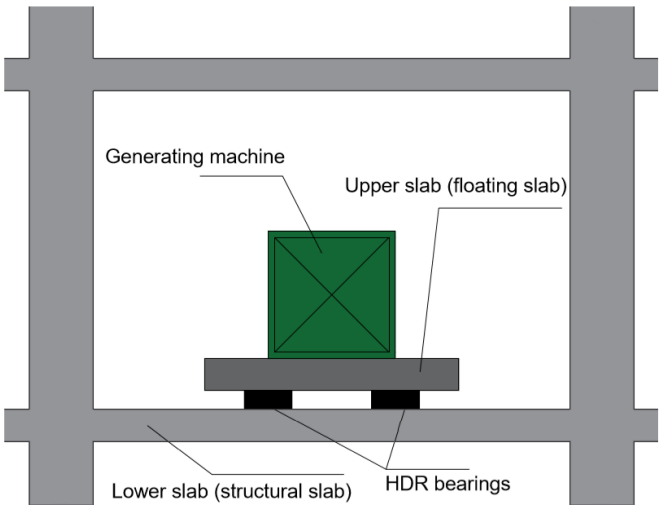

Fig. 6 Installment of FRCISS and generating machine in story floor

A nodal point is the intersection of the regions in the plate that lie between the positive and negative vibration deformation (zero deformation) of the last two shape modes. This technique is also proved to be applicable in the finite element software by applying different frequencies on a plate and following the same steps of the experiment (Hui and Ng, 2007). These points represent the optimum locations for bearings to isolate vibrations on the slab. Therefore, the finite element model of considered slab has been developed using ABAQUS commercial software and slab response under applied load in various modes of vibration has been evaluated. The upper slab is simply supported on the four edges and the resulting shape modes are detected.

A modal analysis with natural frequency step is conducted over the floating slab layer with 10 shape modes. Modes 8 and 9 of the response which resulted at 386.27 Hz and 517.13 Hz natural frequencies, respectively, were the last two symmetrical shape modes and their contour plot graphs (Fig. 8, a and b) revealed the transition regions of zero deformation (colored in blue). The combination of the blue regions of the two shape modes creates four nodal points (in red circles) which are positioned at quarter the span of the plate from each edge (Fig. 7, c) and highlight the optimum locations of the rubber bearings.

2.3. FRCISS Layout and Detailing of Specimens

Following to the optimum location method explained in the previous section, four square-sectioned high damping rubber bearings were placed below the upper floating slab panel under the four corners. Each bearing is located where their center-points intersects with the nodal points of the upper slab panel. Two dynamic testing scenarios will be conducted on the FRCISS specimen; horizontal cyclic testing and vertical half-cyclic testing. Two FRCISS identical specimens are designed for the two testing cases; namely: HC and VC for the horizontal testing and vertical testing, respectively.

Due to limitations in the experimental laboratory, the size of the upper layer for both specimens HC and VC is smaller than lower layer in order to give enough space to the upper slab to displace laterally. Since the upper slab dimensions are designed as 800 mm x 800 mm in plan, the center-point of each rubber bearing were placed at 200 mm from each slab edge. Upper and lower slab layers are designed with accordance to ACI-318-08 and EC2.

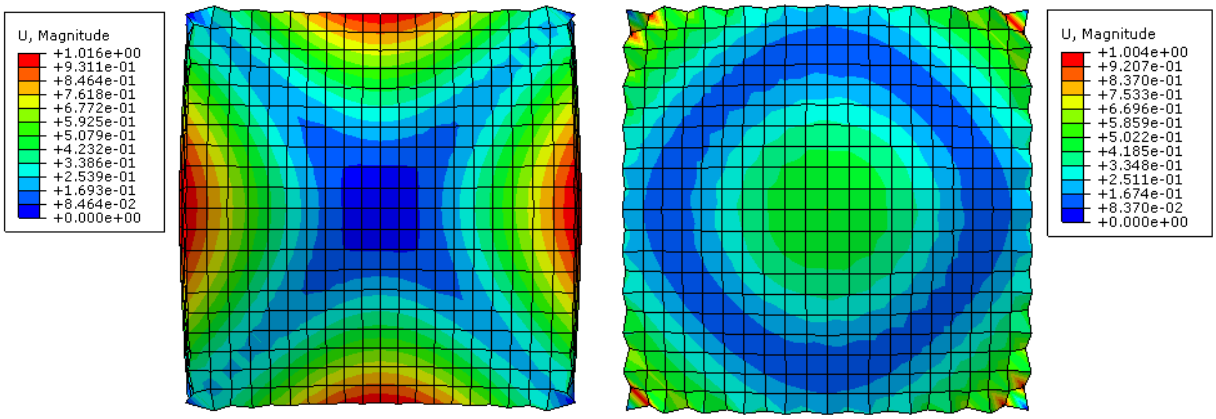

(a) Mode 8 at f_n = 386.27 Hz (b) Mode 9 at f_n= 517.13 Hz

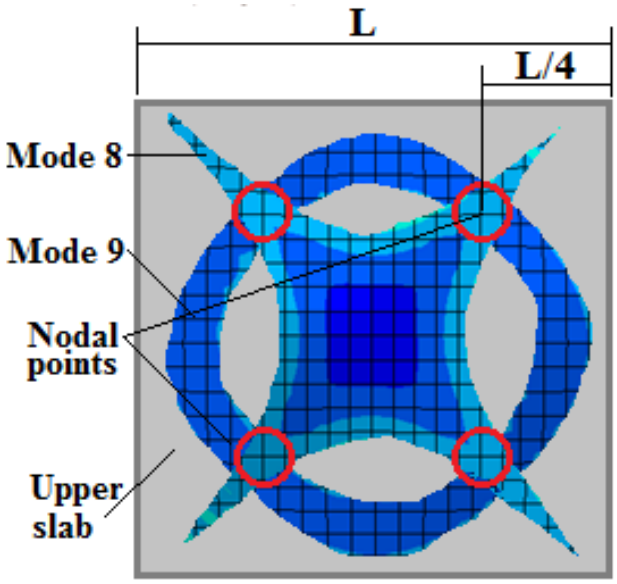

(c) Nodal points formation at the intersection regions of zero deformation of shape modes

Fig. 7 Natural frequency test via FE on upper slab revealing the two symmetric shape modes

Details of FRCISS specimen are shown in Fig. 8. Each slab panel is 10 mm in thickness and reinforced with a single layer of longitudinal and transverse Ø10 mm steel rebars at 20 mm from each slab bottom. The HDR bearings are 150 mm x 150 mm in plan and 60 mm in height which result in a shape factor of 0.625 for each bearing. The bearings are covered with steel plates on top and bottom faces, each plate is 340 mm x 340 mm x 10 mm in dimensions and connecting the bearings with the two concrete slab panels.

3. Numerical Simulation

Finite element software ABAQUS is utilized for the numerical modeling of the proposed FRCISS. Firstly, material properties are defined and specimen parts are created and assigned with the materials accordingly. Specimens HC and VC are modeled and tested under horizontal and vertical cyclic loadings, respectively.

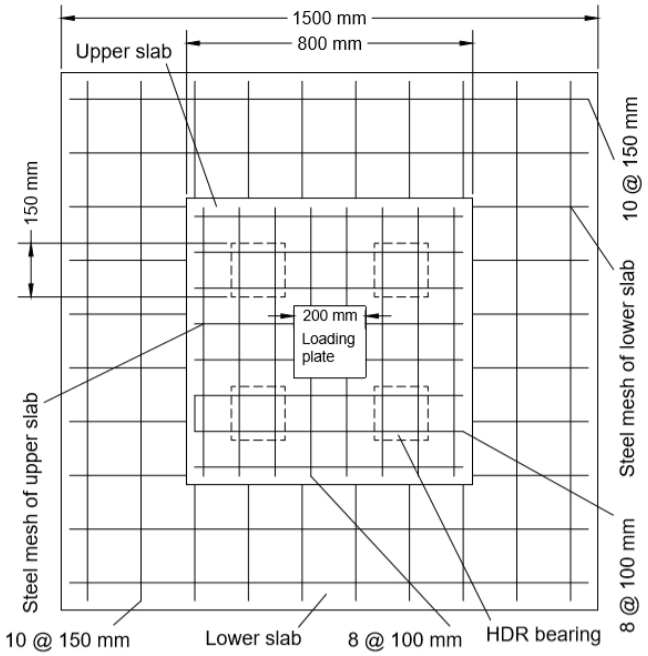

(a) Top view of FRCISS with details

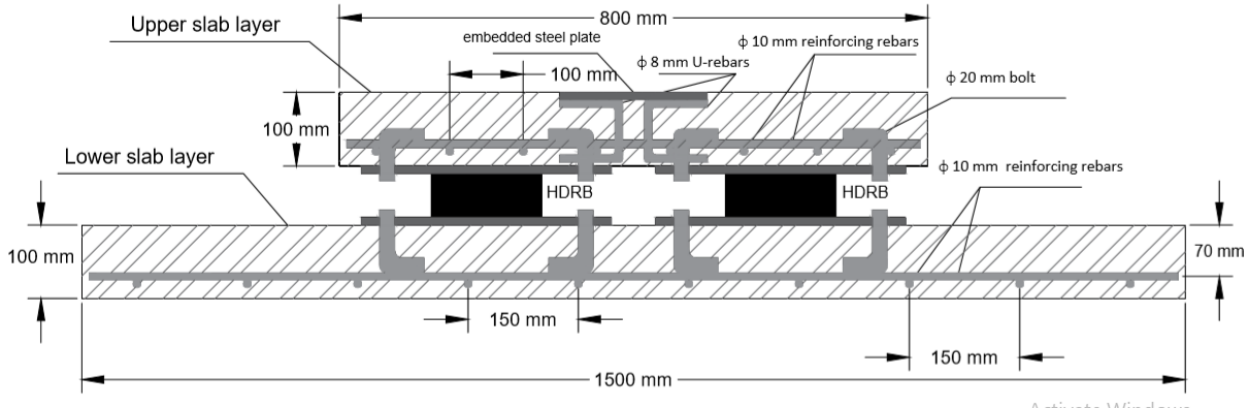

(b) Side view of FRCISS with details

Fig. 8 FRCISS specimen details

3.1. Modeling of High Damping Rubber

High damping rubber (HDR) for the present research is modeled based on experimental test data of previous study conducted by Yoo *et al.*, (1996). It is designed as a hyperelastic material with coefficients of soft compound HDR. The reduced polynomial formula with (N=2) is used since it is stable for all cases.

The test data include: uniaxial, biaxial, planar and volumetric change data (Fig. 9). The experimental results by Yoo *et al.*, (1996) on a circular HDR bearing with steel shims (Fig. 10) were used to validate the finite element HDR model of present work. The cyclic displacement-controlled loading initiated with 50% shear strain up to 400% shear strain. The force-displacement backbone curves of the experimental test of previous work and the numerical test of the FE model show good agreement up to 200% shear strain (Fig. 11), indicating the potential of FE in predicting the HDR behavior in the present research.

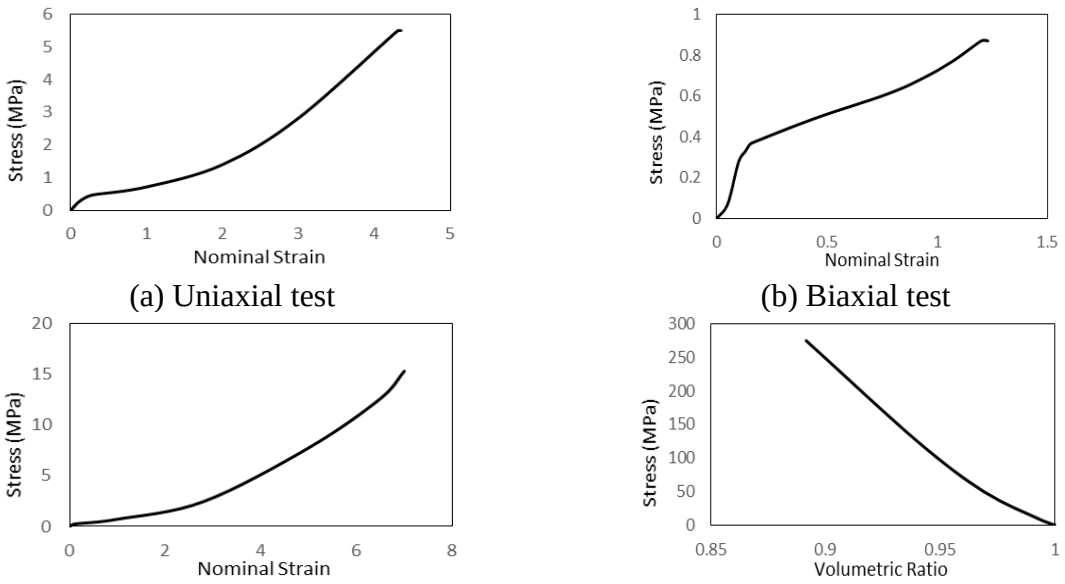

(a) Uniaxial test (b) Biaxial test

(c) Planar test (d) Volumetric change test

Fig. 9 HDR Test Data (Yoo *et al*., 1996)

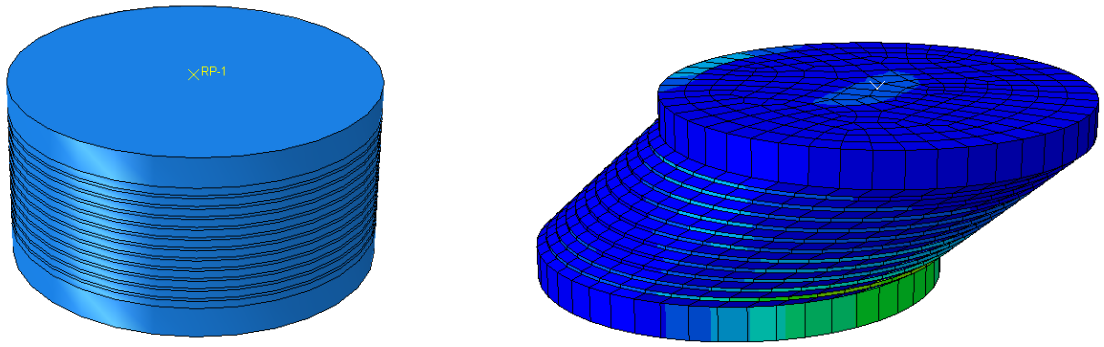

Fig. 10 Soft HDR bearing by Yoo *et al*., (1996) modeled in ABAQUS for validation

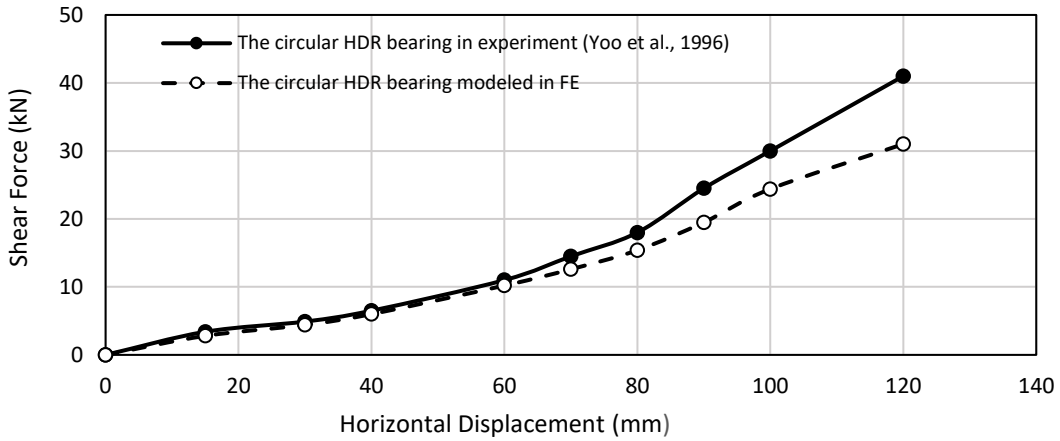

Fig. 11 Shear force-displacement backbone curves for experimental results and FE results

3.2. Modeling of Concrete and Steel

The concrete damaged plasticity (CDP) method was used to simulate the nonlinearity of concrete for the slab panels. Concrete C35/45 is used (Fig. 12). Two types of steel material are designed for reinforcement and plates with yield strengths of 400 MPa and 600 MPa, respectively. Tables 1 and 2 list the properties for both concrete damage plasticity and steel, used in modeling.

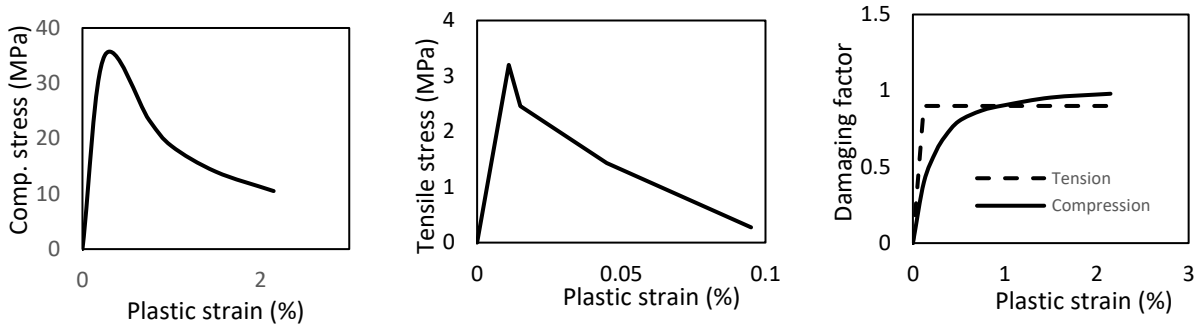

(a) compressive stress-strain (b) tensile stress-strain (c) damaging factors

Fig. 12 Behavior of Concrete C35/45

Table 1 Properties of Concrete

Concrete C35/45			
Elasticity: Elastic		**Mix Design**	
Density (kg/m^3)	2500	**Material**	**Mass (kg) per m^3**
		Cement	400
Young's modulus of Elasticity, E (GPa)	34	Coarse aggregate	1006
Poisson's Ratio, ν	0.2	Fine aggregate	800
		Water	180
		Superplasticizer	2
Plasticity: CDP			
Dilation Angle	30		
Eccentricity	0.1		
fb0/fc0	1.16		
K	0.6667		
Viscosity Parameter	0		
Compressive Strength (Cube) (MPa)	45		
Mean Tensile Strength (MPa)	3.2		

Table 2 Properties of Steel

Steel Properties	Reinforcement Steel	Plates Steel
Density (kg/m^3)	7850	7800
Young's Modulus of Elasticity, E (GPa)	210	200
Poisson's Ratio, ν	0.25	0.2
Yield Strength (MPa)	600	400

3.3. Test Specimens Assembly, Boundary Conditions and Load Application

In both specimens HC and VC, a 3D homogeneous part with C3D8R element type has been used to create the concrete slab layers, bearing covering plates, loading plate, and supports. Whereas, a 3D homogeneous part with C3D8H type element has been used to create HDR bearings.

A wire type part was used to create reinforcing rebars with T3D2 element type for meshing. The slab layers are assigned with the concrete material designed with CDP approach and the steel mesh in both specimens is embedded inside each slab panel 75 mm from the top by using embedment constraint in the interaction tool (Fig. 13).

Furthermore, load plates are tied to the top face of the upper slab layers in each specimen to be displacement-controlled loaded in the test procedure. HDR bearings are connected to steel covering plates which in turn are connected to the slab layers above and below the bearings. Table 3 illustrates the dimensions and number of bearings in each test specimen while Fig. 14 illustrates simulated specimens HC and VC.

For both dynamic testing scenarios, initial and dynamic steps are defined for the boundary conditions set on the two models. In each test, field and history outputs are defined to obtain the targeted results. For the lateral displacement-controlled loading test, the composite model is fixed at the bottom layer on the four edges by restricting translations and rotations in the three dimensions. Afterwards, cyclic protocols are applied to reference points that are assigned to the loading plates to resemble the actuator movement.

In case of horizontal loading test, the loading plate is tied to the upper slab layer via connect tool to resemble the pushover and pullover stages of the horizontal actuator. According to ACI (Robertson and Johnson, 2004), each cycle level was repeated three times to evaluate the loss of stiffness after repeated loading of the structure, and to induce the type of damage expected in a seismic excitation. The horizontal vibration initiates with 5 mm increment and increases by 5 mm each three cycles until reaching a maximum 60 mm horizontal displacement which results in 100% shear strain for the 60 mm high HDRBs (Fig. 15).

Table 3 Number and dimensions of rubber bearings for floating panels under horizontal and vertical vibration

Test No.	Specimen Name	Number of Bearings	Side Length of Bearing (mm)	Height of Bearing (mm)	Shape Factor
Horizontal	HC	4	150	60	0.625
Vertical	VC	4	150	60	0.625

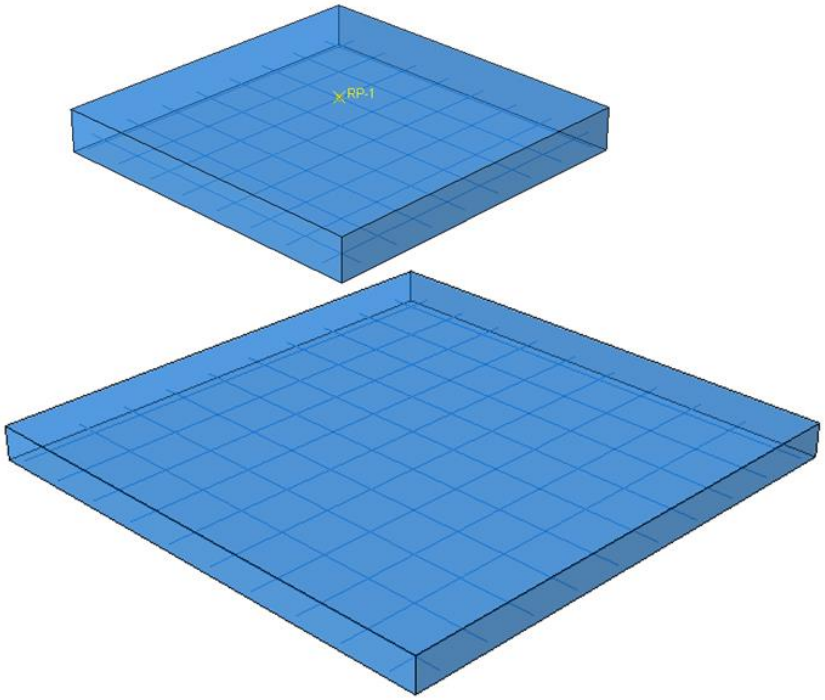

Fig. 13 Upper and lower slab layers with embedded reinforcement

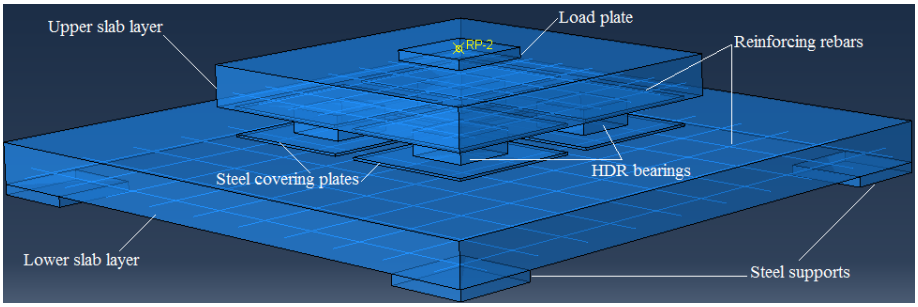

(a) Specimen HC with element meshing

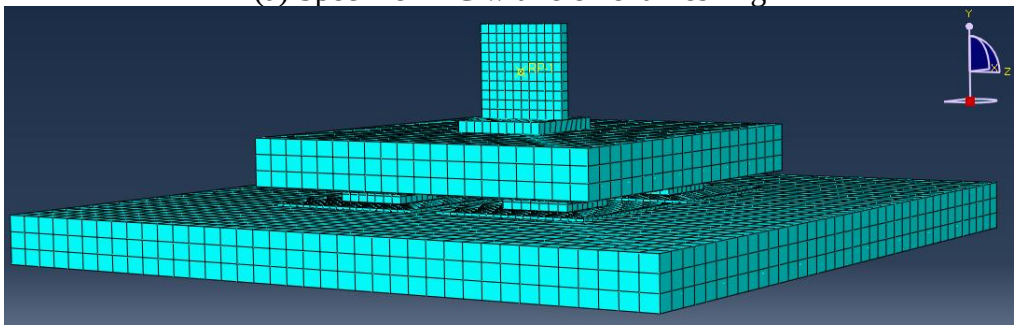

(b) Specimen VC with details of reinforcement, HDR, and slab layers

Fig. 14 FE simulation of specimens HC and VC

Whereas in vertical loading specimen, the loading plate is in contact interaction with the slab layer in order to mimic the real movement of pushover and release of the vertical actuator. Half cycles have been used instead of full cyclic amplitudes and the number of cycles of each amplitude was referred to ACI (2001) and the half-cycle displacements were pressed and released to simulate the real condition of heavy rotary machine on slab panel. The vertical displacement is pointing downwards in the compression direction starting at 2 mm with 2 mm/cycle increment rate down to maximum vertical displacement of 40 mm, which represents two thirds of the compression strain of the HDRBs (Fig. 16).

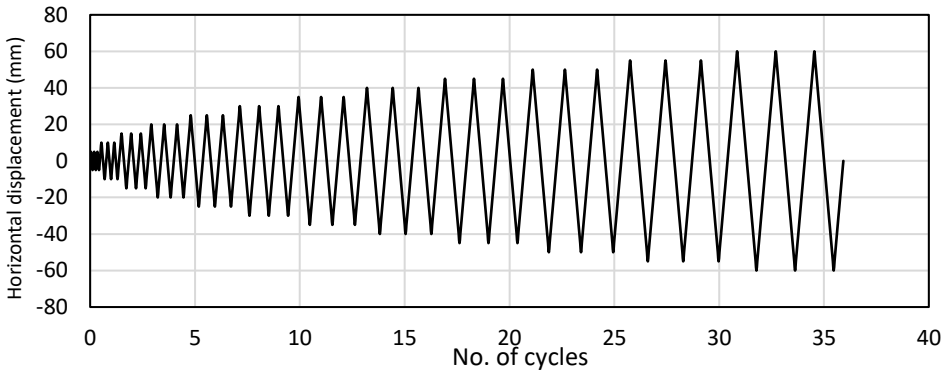

Fig. 15 Horizontal cyclic protocol

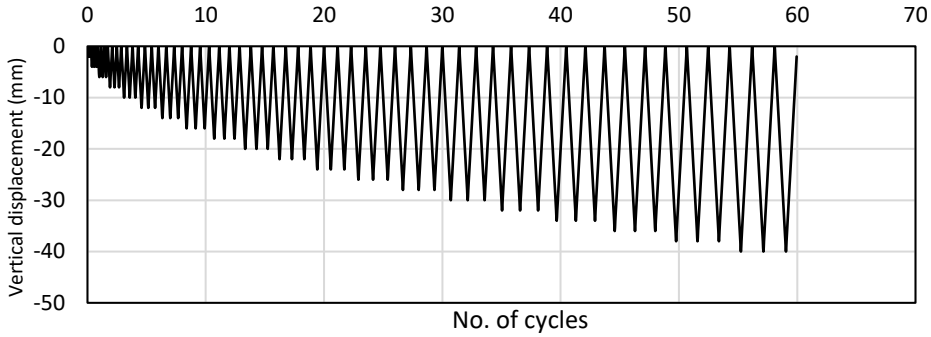

Fig. 16 Vertical half-cyclic protocol

3.4. Numerical Results

3.4.1. Horizontal Cyclic Results

Fig. 17 shows specimen HC with the HDR bearings deformed laterally under the cyclic horizontal loading. Finite element results of specimen HC revealed that the soft HDR bearings provided sufficient amount of flexibility between the two concrete slab layers which is resulted from the low shear stiffness.

A hysteretic behavior in loops form which is generated by the force-displacement axes. This occurred due to the pushing and pulling of the floating slab horizontally as the reaction force degrades during the pulling for a specific displacement compared to the pushing (Fig. 18). The effective shear stiffness, $K_{h.eff.}$, in each loop is taken as the maximum force divided by the peak horizontal displacement of the that loop. The shear stiffness is seen large at the beginning of the test, which can be beneficial in resisting low amplitude vibrations such as low-mass rotary machines-induced vibrations. It initiates with 0.87 KN/mm then it drops gradually with the

increment in horizontal displacement of the rubber bearings up to 60 mm displacement (100% shear strain) to 0.27 KN/mm with a slight augmentation at 25% shear strain in the positive and negative directions (Fig. 19). This offers enough flexibility to reduce vibrations in the shear direction.

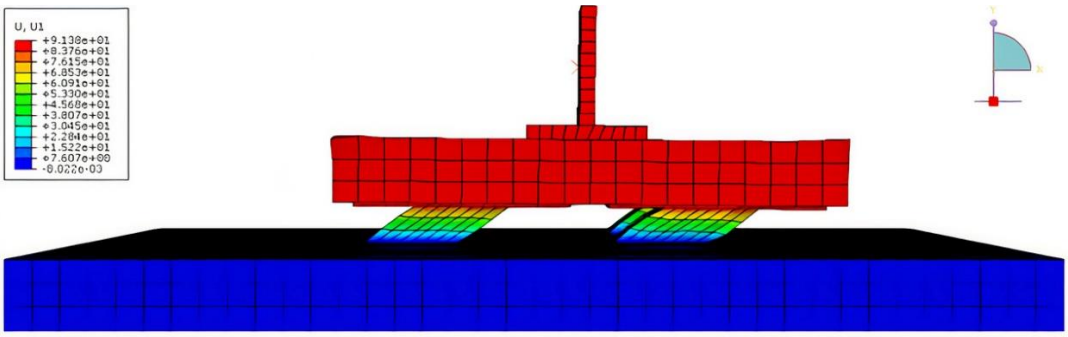

Fig. 17 Deformation of specimen HC under horizontal cyclic loading

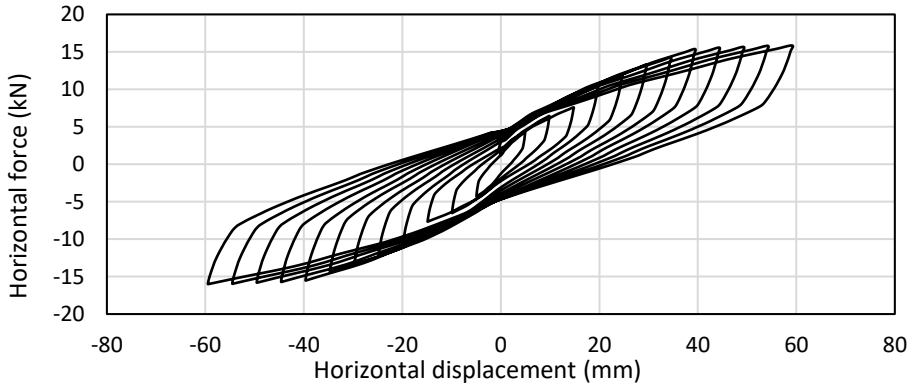

Fig. 18 Force-displacement hysteretic loops behavior of specimen HC under horizontal cyclic loading

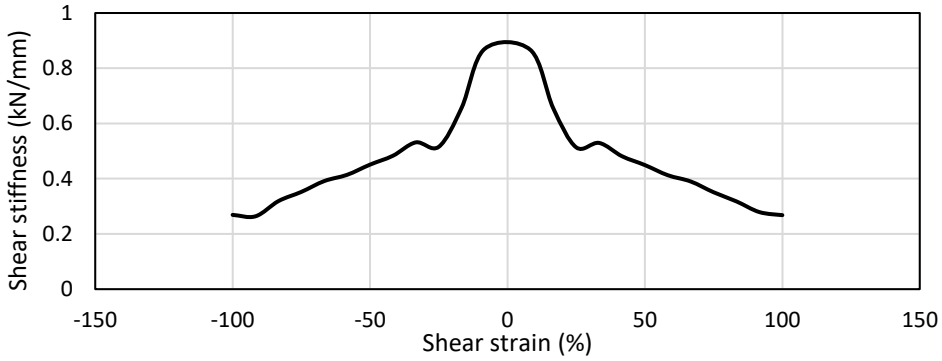

Fig. 19 Shear stiffness vs. shear strain of HDR bearings

3.4.2. Vertical Half-Cyclic Results

Fig. 20 demonstrates specimen VC under compressive loading which causes the rubber bearings to bulge laterally. Unlike specimen HC, numerical testing of specimen VC under half-cyclic loading showed a much distinct performance.

The hysteretic loops have disappeared, meaning the force is restored during the release stage of the test. Fig. 21 shows that the relationship between compressive force and vertical displacement is almost linear which indicates a constant compressive stiffness throughout the test. On the other hand, deflection which was measured in the midpoint and at one fourth of the lower slab span from each side, showed a 28.8% decrement compared to the vertical displacement applied on the upper slab (Fig. 22). This is a result of HDR bearings providing low average compressive stiffness of 1.44 KN/mm which mitigated vibrations on the lower slab and minimized deflections.

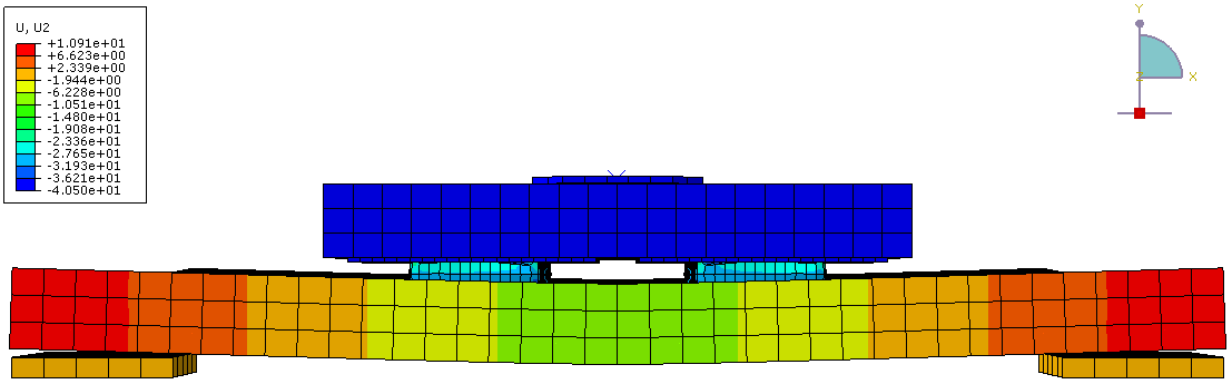

Fig. 20 Deformation of specimen VC under vertical half-cyclic loading

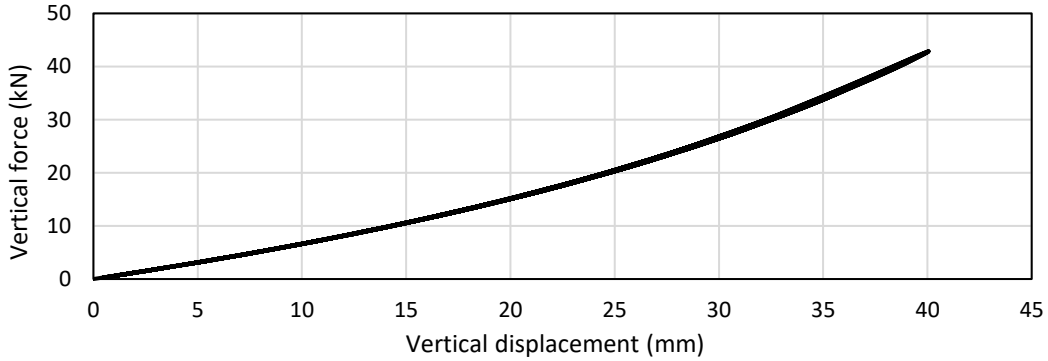

Fig. 21 Force-displacement behavior of specimen VC under half-cyclic vertical loading

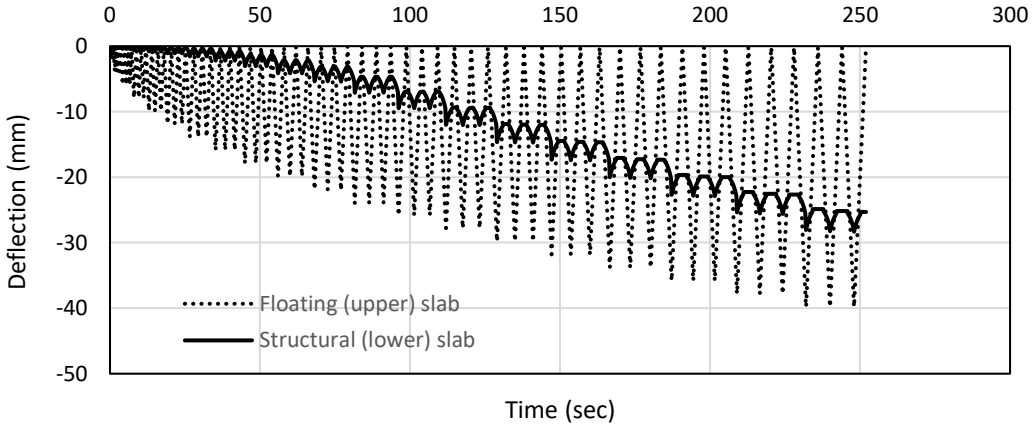

Fig. 22 Deflection at midpoint in control specimen and lower slab of specimen VC under half-cyclic vibration

4. Experimental Work

For validation of FE simulation, FRCISS specimens HC and VC should be experimentally tested. The elements that construct the specimens should be designed and fabricated and then assembled accordingly.

4.1. Fabricating and Casting

Size and height of the HDR bearings are based on design calculations of shear stiffness, K_h and compression stiffness, K_v values by Sunaryati *et al*., (2008). The same specimen dimensions of the FE simulation are adopted in the experimental work.

The bearings which compose HDR are linked thermally to the steel covering plates on top and bottom. The four HDR bearings are connected to the slab layers by Ø20 mm steel bolts that have been already embedded in the concrete during casting of specimen. Steel shims are absent in the rubber in both specimens in order to reduce the compressive stiffness of the bearings (Fig. 23).

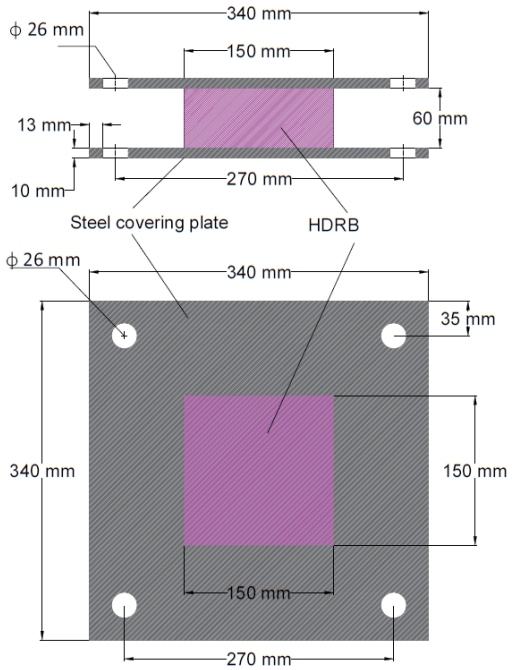

Fig. 23 Side view and top view of rubber bearing for half-cyclic compression test

Slab layers, on the other hand, are casted by pouring concrete into wooden molds. In each mold, longitudinal and transverse bars were placed and welded together to form a mesh. The reinforcement of the upper slab (for horizontal testing) is placed 25 mm from the top face of the mold during the casting of concrete since it will be flipped upside down when it's connected to the rubber bearings and will be located at 25 mm from the bottom face of each slab layer during the two testing procedures. Fig. 24 shows the reinforcement in the wooden mold before casting in each slab layer.

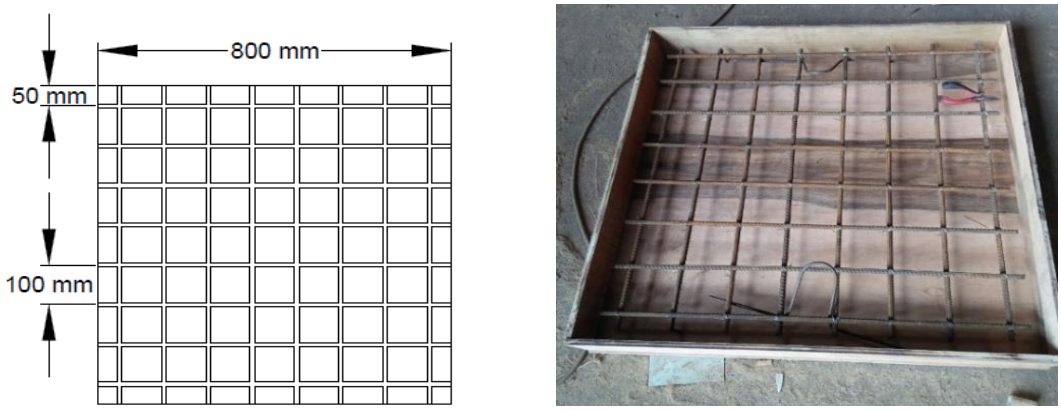

(a) upper slab reinforcement

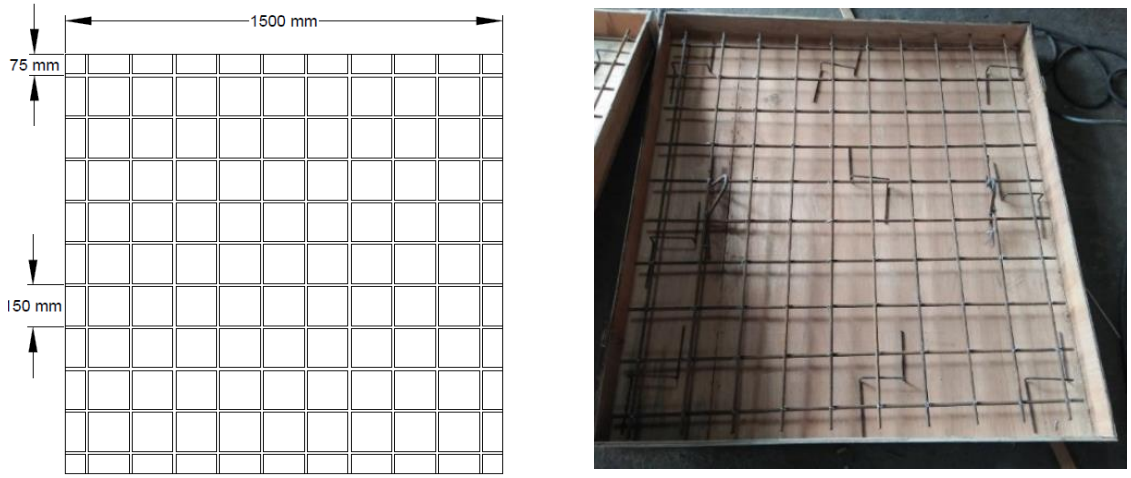

(b) lower slab reinforcement

Fig. 24 Details of steel mesh

A 300 mm square steel plate with 10 mm thickness is tied to the top face of the upper concrete slab layer during the casting process and connected to the steel mesh layer via U-shaped steel bars that are welded to both the steel plate and the mesh, as the upper layer will be flipped upside down to be tied above the lower layer. This plate will be connected to a steel I-beam which in turn is connected to the horizontal actuator before the test. In addition, Ø20 mm steel bolts are bent to be L-shaped and welded to the steel mesh pointing upwards in each slab for the lateral displacement test specimen and extending 20 mm out of the slab surface to pass through the holes in the steel covering plates of the HDR bearings and be tied with them.

Moreover, four plastic tubes with 50 mm diameter and 150 mm height are placed at the corners of the mold with 100 mm distance apart from each other to create 50 mm holes for fixing the lower slab to the strong floor via Ø50 mm bolts during the test (Fig. 25). However, for the vertical displacement test, bolts are omitted since the rubber bearings undergo vertical motion which prevent any slab lateral movement over the rubber bearings. A loading plate is placed on top of the upper slab to transfer and distribute the vertical actuator force to the upper slab.

Fig. 25 Steel bolts and load plate embedded inside upper slab for horizontal test before casting

4.2. Material Properties

Tables 4 and 5 list the properties of concrete, steel rebars and HDR, respectively. Whereas, high-tensile steel reinforcing rebars were used to reinforce the concrete slab panels. Since the slab panels are designed for vibration machinery of low mass compared to structural buildings, soft compound high damping rubber of shear modulus, G (0.4 – 0.6) MPa is selected for the design of the bearings (Naeim and Kelly, 1999)

Grade C35/45 concrete was used to cast the slab layers. Cubic and cylindrical samples were taken from the mixture, (Fig. 26) and tested during the casting. The samples were tested in different time periods; 7, 14, and 28 days of curing and the average compressive strength values are listed in Table 4.

Table 4 Concrete and Steel Rebars Physical Properties

Properties	**Concrete**		**Steel rebars**
Density (kg/m^3)	2500		7850
Compressive cube strength, f_{cu} (MPa)	7 days	37.15	-
	14 days	41.61	
	28 days	46.94	
Yielding strength, f_y (MPa)	-		597
Ultimate tensile strength, f_u(MPa)	-		677
Tensile strength, f_t(MPa)	3.2		-
Young's modulus, E (GPa)	34		210

Table 5 Physical HDR Properties

Type	Shear Modulus (MPa)	Tensile strength (MPa)	Elongation at break (%)	Tear resistance (KN/m)
Soft	0.4 – 0.6	≥ 13	≥ 400	≥ 7

Fig. 26 Cubic concrete samples for compressive strength test

4.3. Test Setup and Cyclic Loading Protocols

Two dynamic actuators comprise MTS and Shimadzu dynamic actuators with 300 KN load capacity (Fig. 27), implemented to test the dynamic response of the proposed FRCISS specimens in vertical and horizontal directions. The two specimens; HC and VC were prepared.

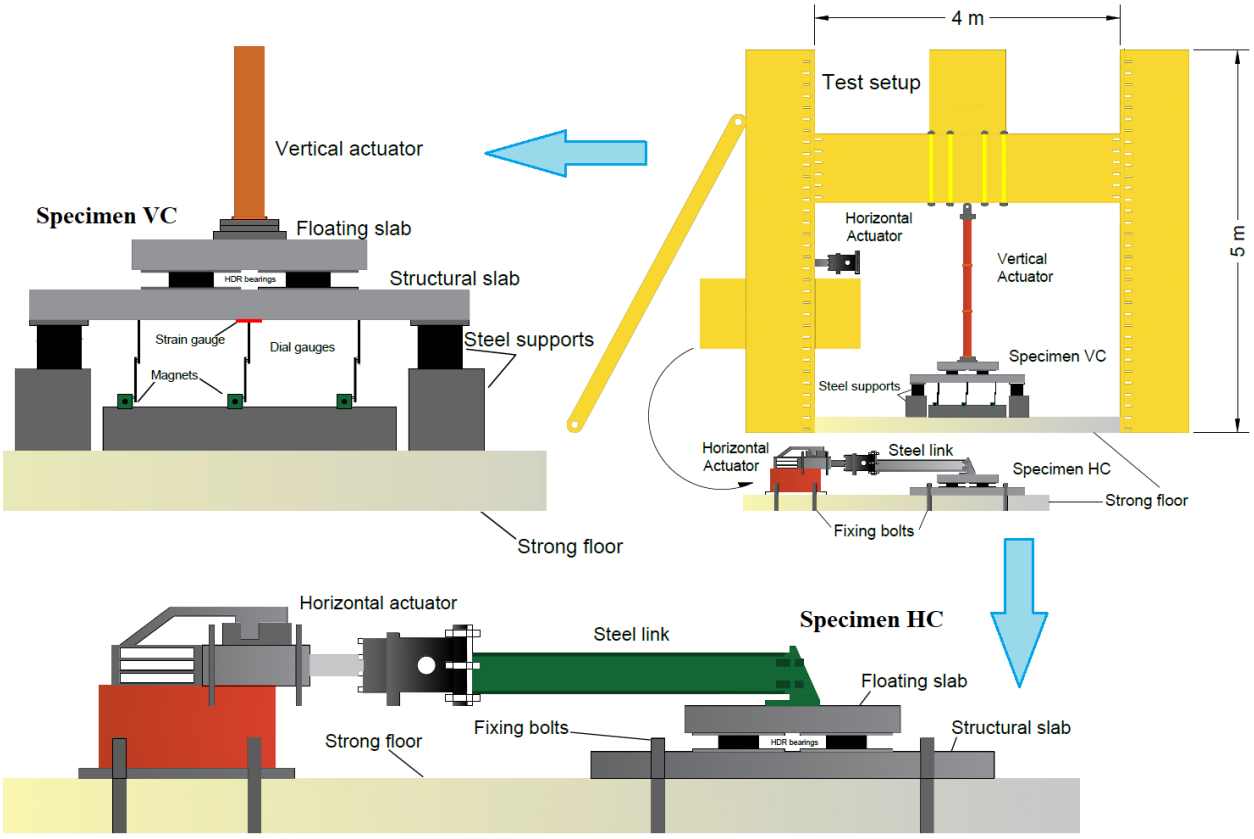

Fig. 27 Test setup layout for specimens HC and VC

The lower slab of specimen HC is fixed to the strong concrete floor via 50 mm steel bolts that extend 100 mm above the lower layer top face. Thus, the dimensions of upper layer are minimized in order to avoid the contact with the bolts during the lateral pushover and pullover phases.

The horizontal actuator is connected to the top face of the upper layer by a steel link with I-section beam and 2 plates; one is bolted to the actuator and the other is bolted to the perpendicular plate that is connected to the top of the slab panel. Whereas, the specimen VC is supported at the four corners on steel supports of 200 mm x 200 mm plan and loading is applied on a steel plate contacting with the top face of the upper slab layer. The same cyclic loading protocols in Figures 15 and 16 are applied on the test specimens HC and VC experimentally; a horizontal cyclic displacement-controlled loading test and a vertical half-cyclic displacement-controlled loading test to imitate a 3-D vibration pattern of an actual machinery system.

4.4. Validation of FE Simulation with Experiment

4.4.1. Horizontal Testing Validation

Fig. 28 demonstrates specimen HC under the horizontal cyclic loading conducted by the horizontal actuator in the laboratory. The test results of specimen HC agree well with the FE results. The backbone curves of both tests match almost perfectly for most of the shear cycles except at large cycles that are approaching two thirds of the shear strain of the HDR bearings (Fig. 29). The difference in hysteretic first loop resulted from the experimental test and analysis as showed in Fig. 29 b, is 17.8%.

First crack is reported at a horizontal displacement of 45 mm that corresponded to a 14.8 KN shear reaction force and a degradation in shear force followed that, both in positive and negative directions during pushing and pulling phases, respectively, until total failure occurred when the steel loading plate separated from the surface of the upper slab panel. This is due to the shear punching in the concrete upper layer in the region where the embedded loading steel and the horizontal steel link are connected (Fig. 30). It may have occurred due to the small thickness of the steel plate which led to the disconnection.

Shear stiffness, which is calculated for the peak force-displacement of each cycle is almost as well, compatible for the experiment and FE tests (Fig. 31).

Notably, the hysteretic loops for the experiment appear smaller in area, which indicates that the dissipated energy is less than predicted by finite element. Fig. 32 shows the similarity in deformation of the HDR bearings under the horizontal loadings for the experimental and numerical testing of HC.

Fig. 28 Experimental testing of specimen HC under horizontal cyclic loading

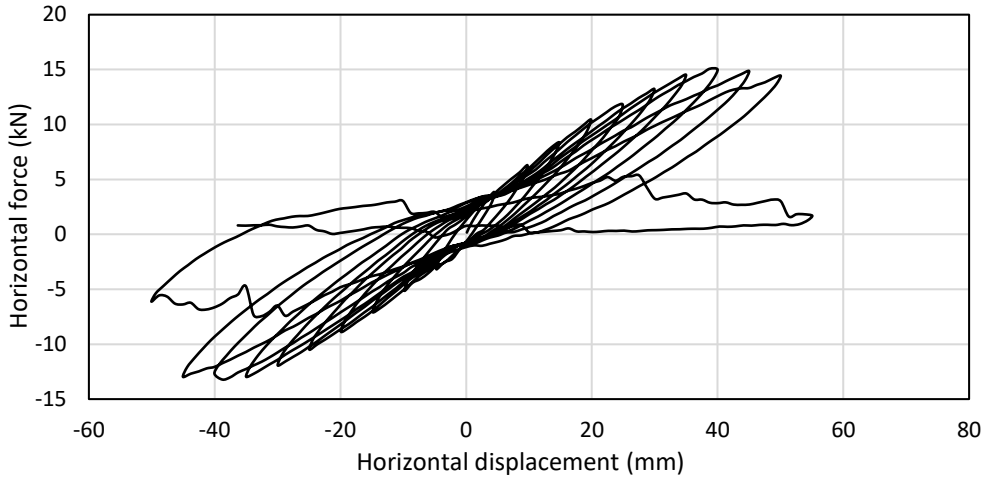

(a) Experimental shear force-displacement relationship of specimen HC under horizontal cyclic displacement

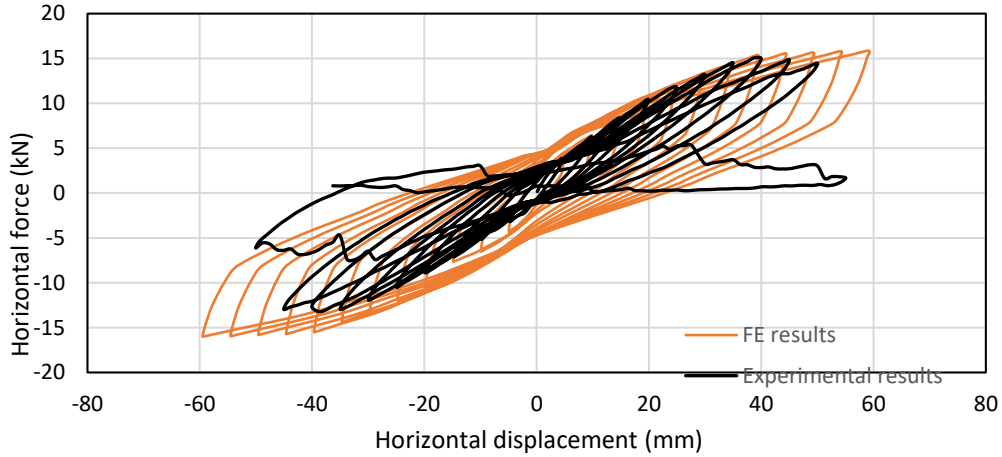

(b) Comparison between the shear force-displacement hysteretic loops for experimental and numerical tests of specimen HC

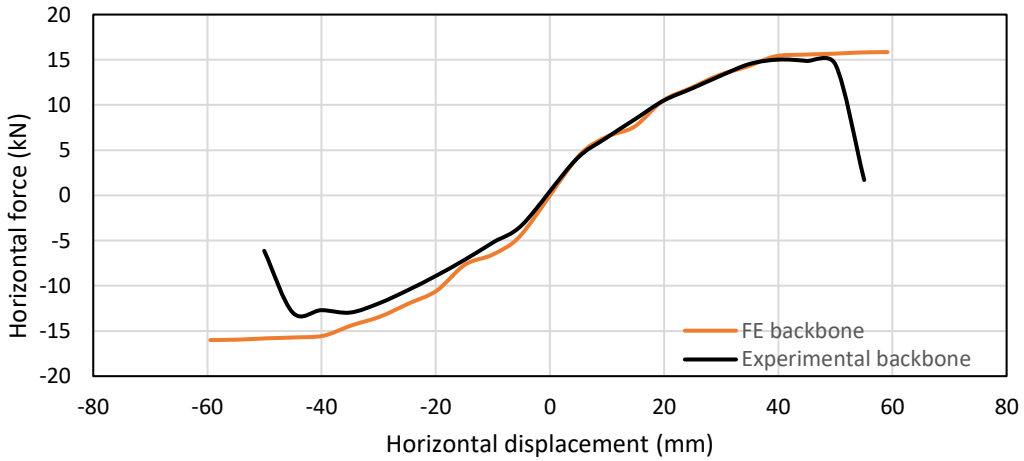

(c) backbone curves of the shear force-displacement curves of FE and experimental HC

Fig. 29 Validation of FE results of specimen HC with experiment

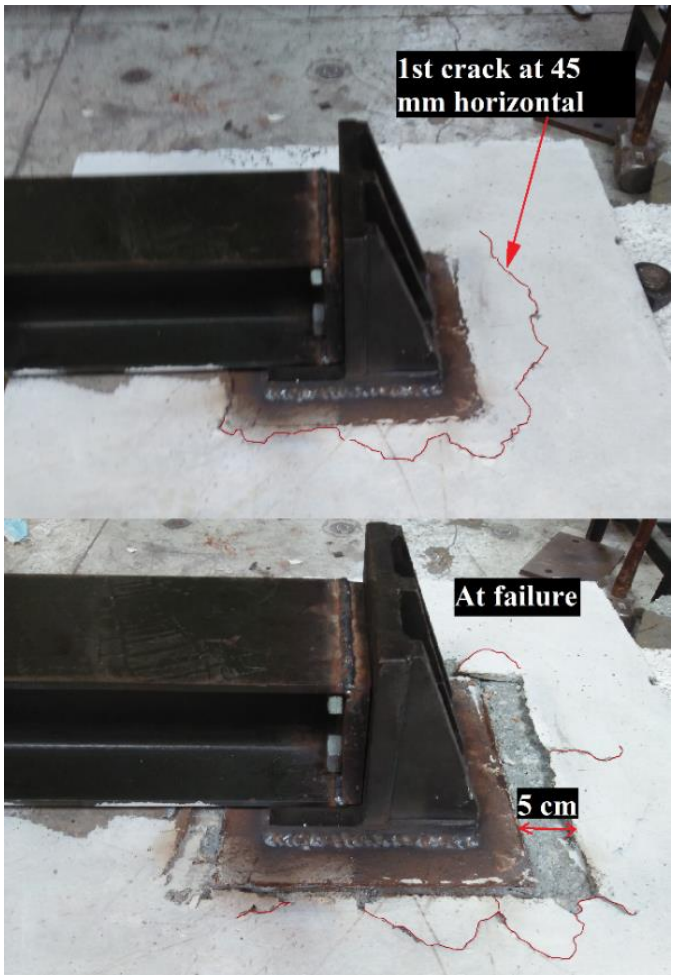

Fig. 30 The shear punching in the upper concrete slab of specimen HC under the horizontal pushing and pulling with first and at failure crack

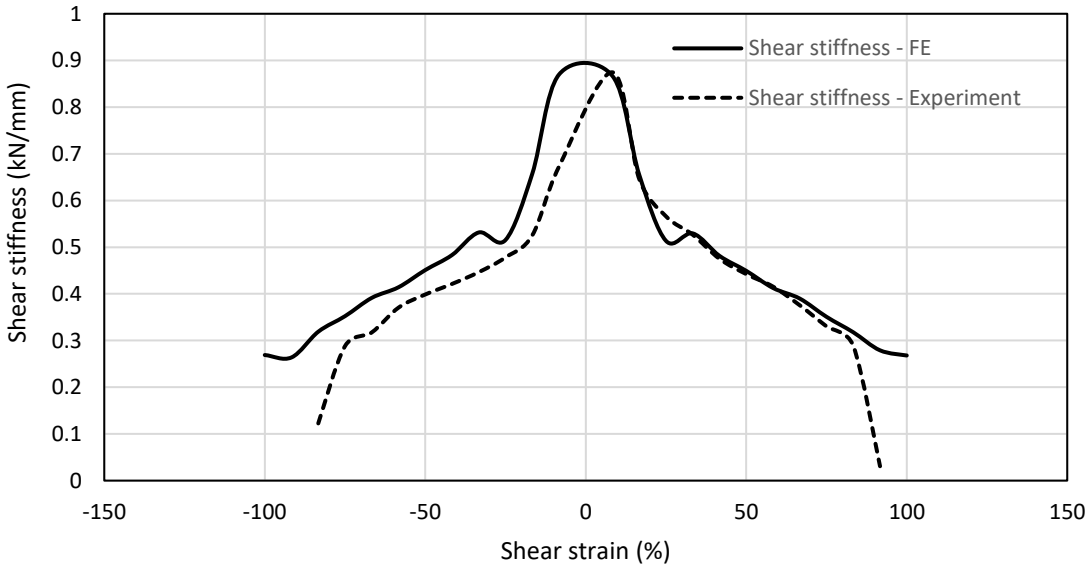

Fig. 31 Shear stiffness of HC calculated for maximum force and displacement of each cycle for the FE and experimental tests

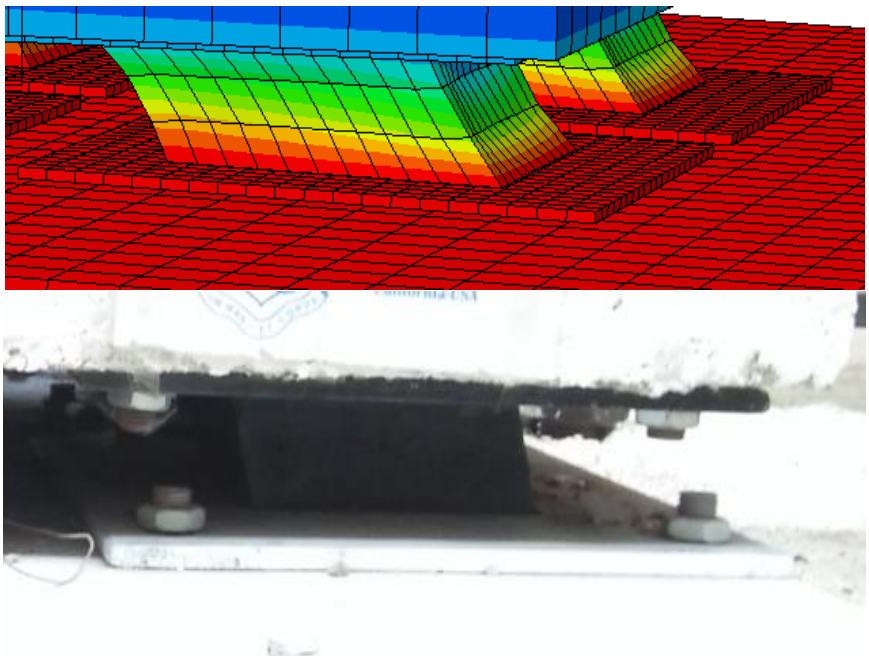

Fig. 32 HDR deformation in experiment and FE simulation for specimen HC

4.4.2. Vertical Testing Validation

Figure 33 shows specimen VC under the vertical actuator. A half-cyclic displacement-controlled loading has been applied on top of the upper floating slab on a steel loading plate, pushing downwards and releasing. The resulted vertical force was almost linear to the respective displacement and reached a 38.2 kN for 40 mm vertical displacement which is 66.67% of the compressive strain of the HDR bearings. First crack occurred in the midpoint of front edge of the lower slab panel at 18 mm vertical displacement, which is equivalent to 15 KN. However, specimen VC did not fail under the designed cyclic displacement, and the failure cracks happened after the post-loading stage, when the specimen was subjected to static load beyond 40 mm. This indicates that the HDR bearings managed to keep the structural slab protected from totally collapsing under the maximum vertical vibration amplitude and the achieved well energy absorption that kept the upper slab from cracking. The dial gauges set under the structural lower slab of the specimen read the displacements under the cyclic compressive loadings. The three gauges gave the deflection of the lower slab in the middle and the quarter the span of the slab in right and left directions (Fig. 34).

Comparison of these results with numerical results shows a great matching between the two tests. Both force-displacement and deflection at different compressive strains agree well (Fig. 35), which indicates the high level of reliability on FE simulation. In Fig. 36 a comparison between the deformation of HDR bearing under compression shows the similarities for actual and simulated testing.

5. Application of FRCISS in 3-Story 1-Bay Building

5.1. Modeling of a Lab-size 3-Story 1-Bay Building

In order to assess the effectiveness of FRCISS in controlling three dimensional vibrations, It's applied in a multistory building. The building is a half scale structure with three stories and one bay each which is taken from a case study building (Robertson *et al*., 2002).

Fig. 33 Experimental testing of specimen VC under vertical half-cyclic loading

Fig. 34 The three dial gauges set under the lower slab

The 3-story 1-bay simulated building is verified by remodeling specimen 1C from a Robertson's research work numerically. The specimen is a lab-size flat slab of reinforced concrete from a flat-plate prototype multi-story building without shear reinforcement subjected to gravity load equivalent to dead load plus 30% of live load.

The prototype building and the test specimen 1C are shown in Fig. 37 while the remodeled 1C is illustrated in Fig. 38. The details of the slab reinforcement with the column and the test setup are shown in (Robertson *et al*., 2002). A horizontal cyclic displacement-controlled loading protocol (Fig. 39) is applied on the top of the upper column and the lower column is pinned to the strong floor while the edges, perpendicular to the loading direction, are restricted in the vertical direction and kept free to move in the horizontal direction.

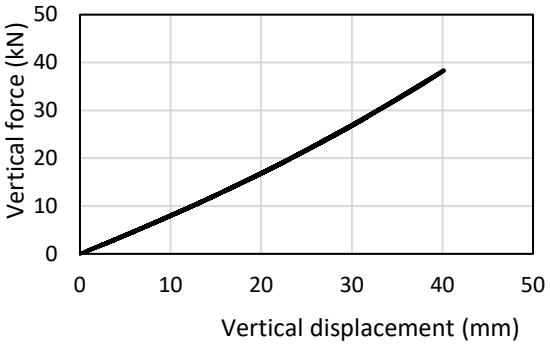

(a) Experimental compressive force-displacement relationship of specimen VC under vertical half-cyclic displacement

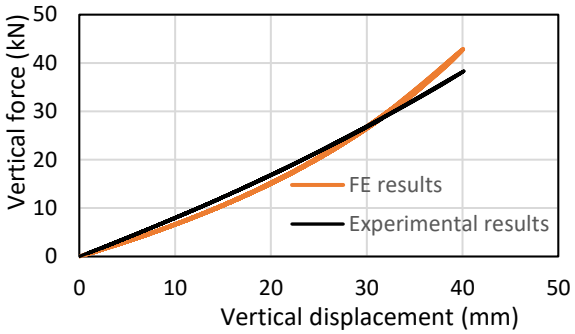

(b) Comparison between the compressive force-displacement for experimental and numerical tests of specimen VC

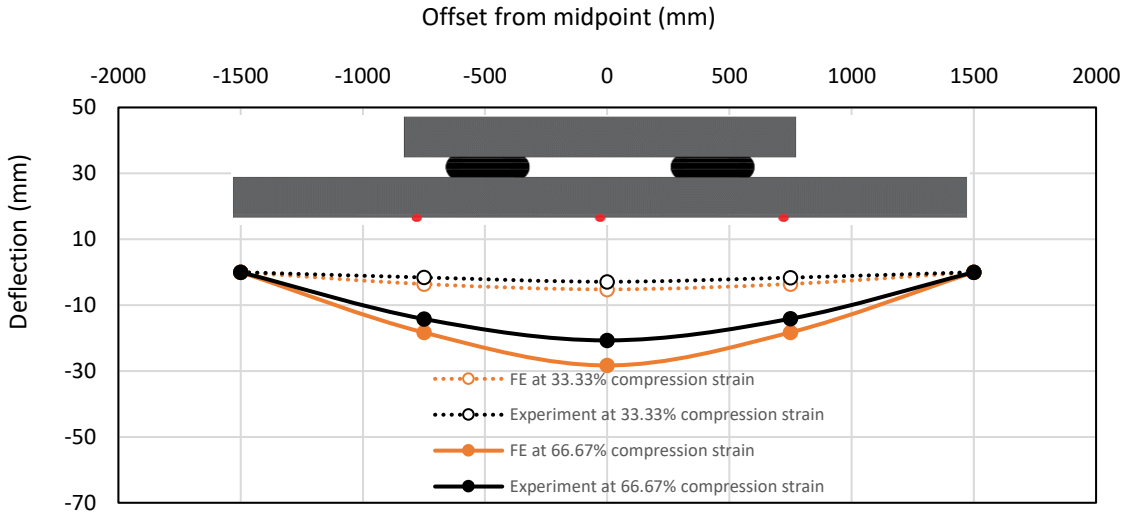

(c) Deflection at midpoint and quarter-point of the lower structural slab of VC in FE and experiment at one third and two thirds of the HDR compression strain

Fig. 35 Validation of VC

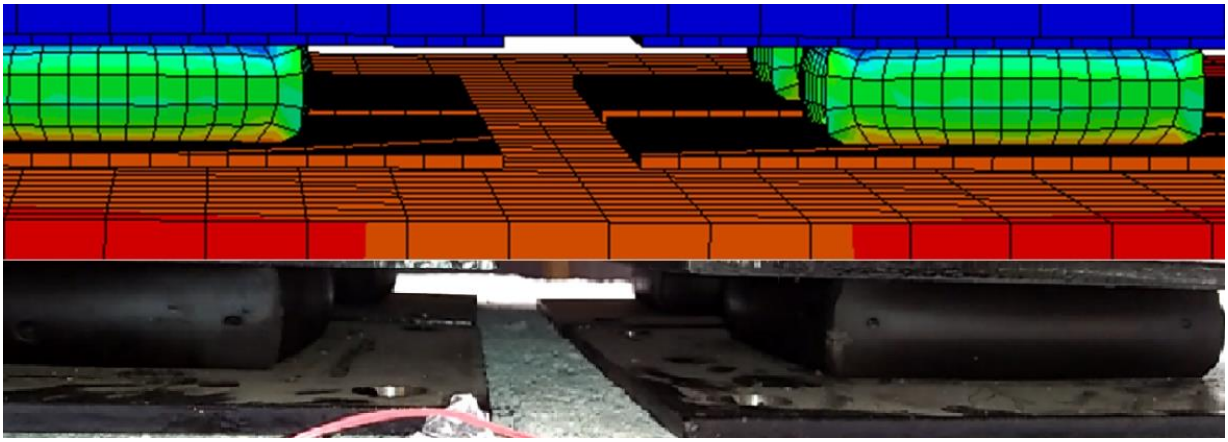

Fig. 36 HDR deformation in experiment and FE simulation for specimen VC

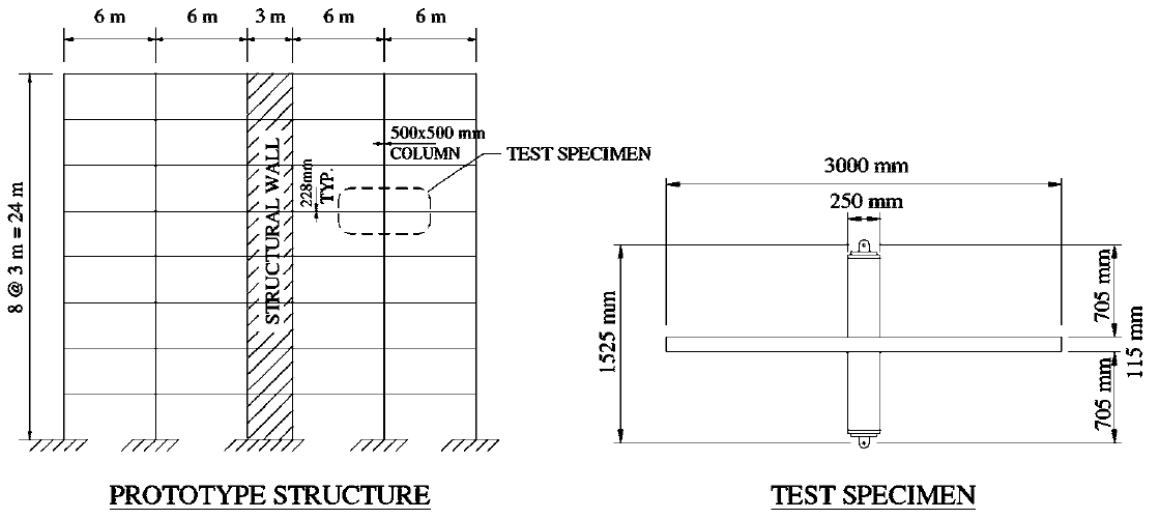

Fig. 37 The prototype building and test specimen (Robertson *et al*., 2002)

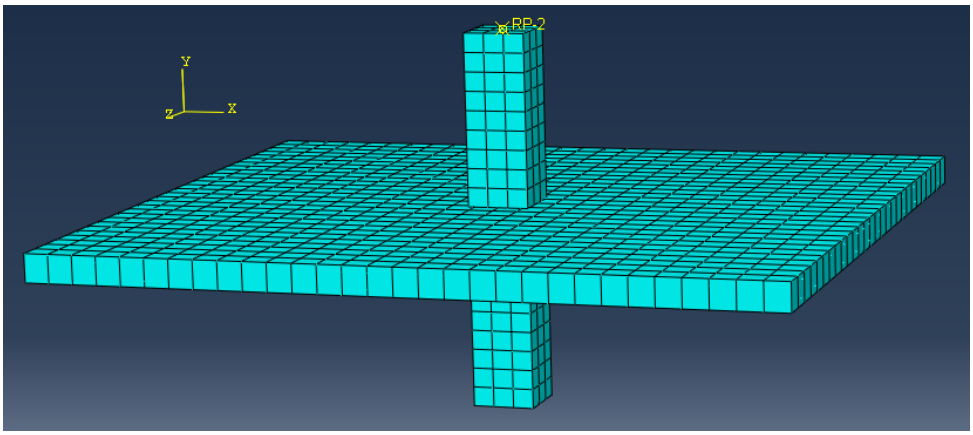

Fig. 38 Specimen 1C with mesh elements remodeled in FE

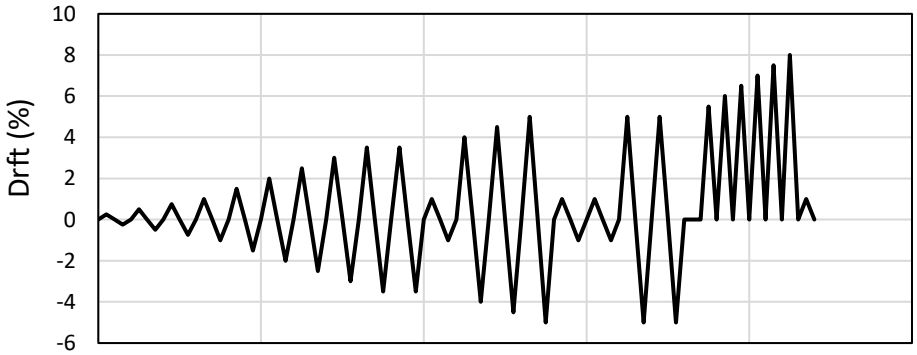

Fig. 39 Cyclic loading protocol (Robertson *et al*., 2002)

Experimental response of the flat slab-column connection under the cyclic vibration is shown in Fig. 40 which illustrates the force-displacement hysteresis of phase 1 of the protocol that peaks at 4% drift. Whereas, the response and backbone curve of FE modeled specimen under the same cyclic protocol is shown in Fig. 41.

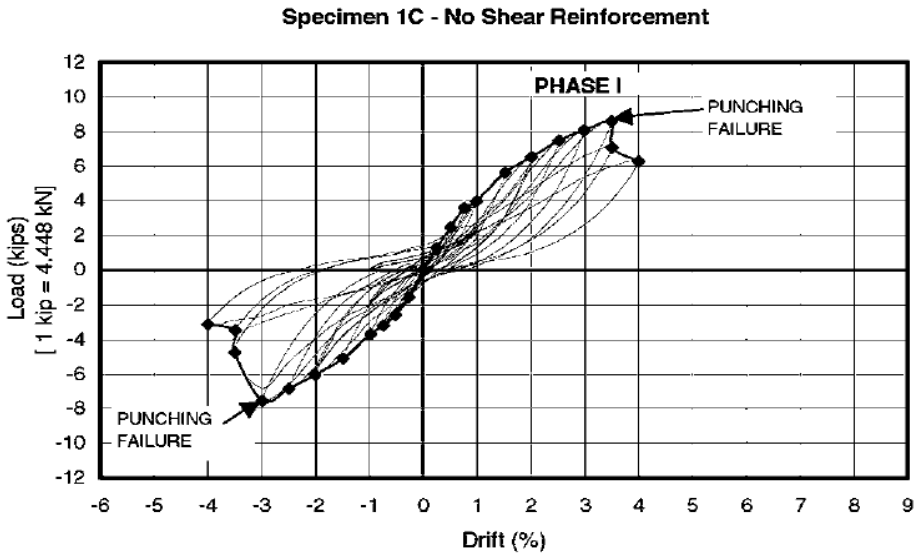

Fig. 40 Hysteretic response and backbone curve for control specimen 1C without shear reinforcement (Robertson *et al*., 2002)

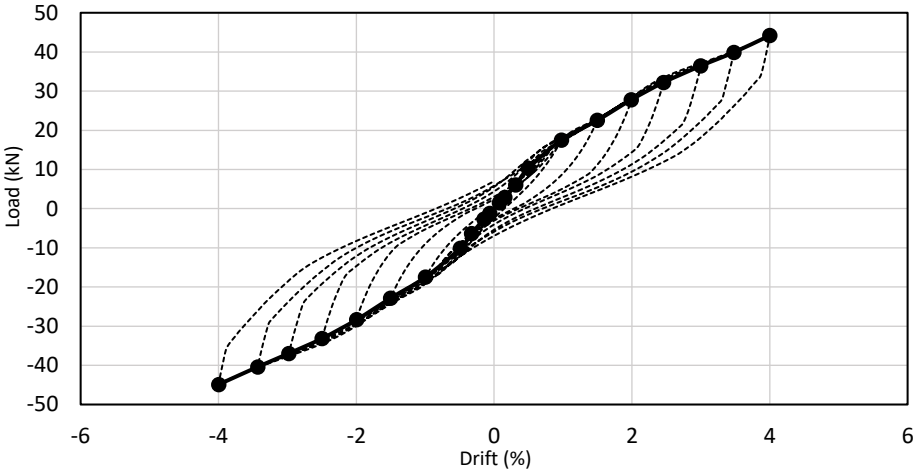

Fig. 41 Hysteretic response and backbone curve for FE model under cyclic protocol phase 1

Result shows a good agreement and a remarkable correlation in the force-drift hysteretic backbone curves of the FE and the experimental tests, except for the punching failure which occurs at 3.5% drift when the force value drops, that the FE model couldn't predict precisely (Fig. 42). However, this will not affect the validation, since punching is out of this research scope. Thus, this model is used in constructing a lab-size 3-story 1-bay structure of a typical building and implementing the proposed FRCISS in the story levels in order to assess its efficiency to reduce deformations and minimize inter-story drifts to the allowable limits.

Hence, the 3-story 1-bay building is numerically modeled. For the evaluation of the FRCISS influence on the overall performance of the multi-story building, a conventional 3-story 1-bay building which doesn't include the installment of the floating system within it has to be tested and compared with the modified building.

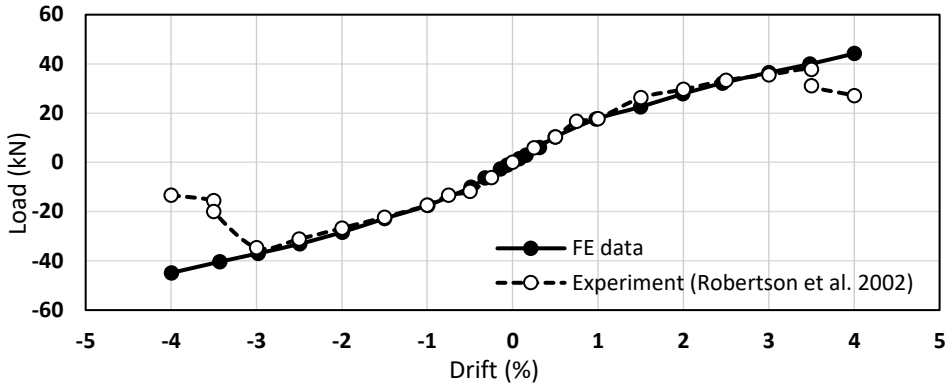

Fig. 42 Comparison between the hysteresis force-drift backbone curves of the original 1C from experiment (Robertson et al., 2002),and the FE remodeled 1C

Three cases for both buildings are studied: 1) the vibration machine is installed in the 1st story; 2) the vibrating machine is installed in the 2nd story; and 3) the vibrating machine is installed in the 3rd story. The vibrating machine is represented by a mass of 5 tons in the modeling of the building. Gravity load is also applied on the whole structure. For the adjusted building, the FRCISS is installed in the middle of the story of the vibrating machine as the latter is attached to the floating slab of the floating system. Dimensions of the building are shown in Fig. 43, and details of the three cases for each type are shown in Fig. 44. The building is composed of 3 m x 3 m RC flat slabs of 110 mm thickness and supposed by four 0.2 m x 0.2 m x 1.5 m reinforced concrete columns. The slabs and columns are considered to be casted without interruption. The building is fixed to the ground by the four columns of the ground level with the boundary conditions of restricted translation in the three dimensions (Ux = Uy = Uz = 0). Table 6 lists the details of the two types of the 3-story 1-bay buildings with the 3 cases of machinery installment of each.

The multistory building 3D deformations will be tested under interior vibrations, induced by the vibrating machines themselves and exterior vibrations, generated by a 3D earthquake.

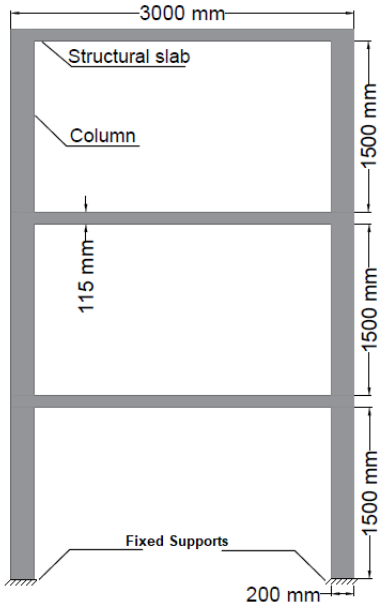

Fig. 43 Dimensions of slabs and columns of the 3-story 1-bay building

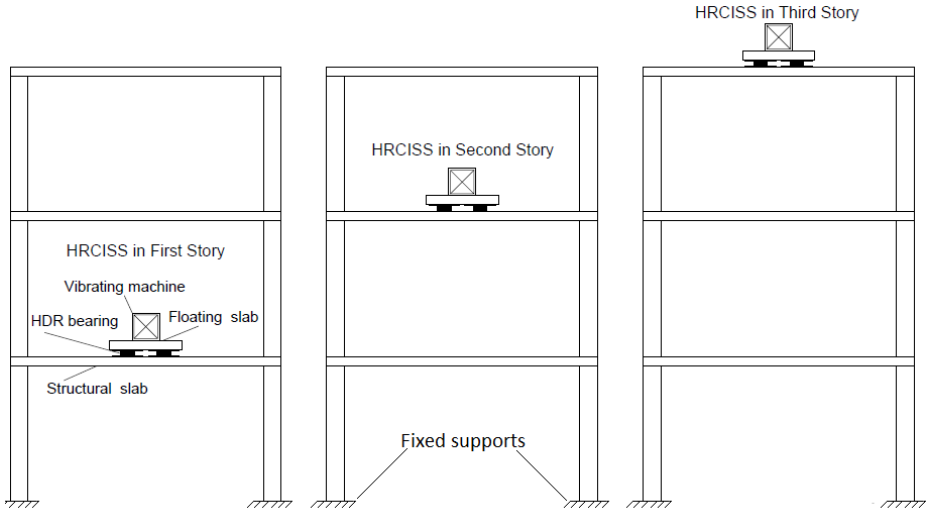

(a) Modified 3-story 1-bay with vibrating machine installed in first, second, and third story (b)

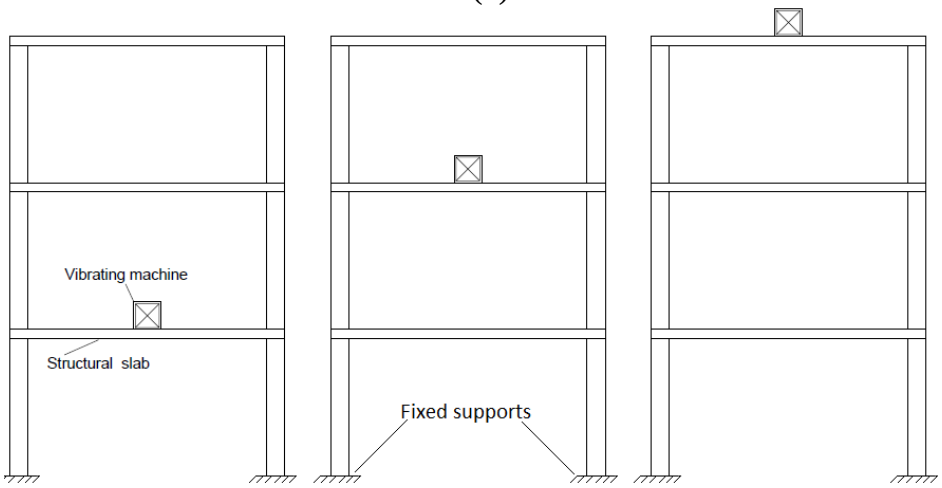

(b) 3-story frame, 1-bay with vibrating machines installed in first, second, and third stories

Fig. 44 Modified and conventional 3-story 1-bay buildings: (a), and (b)

Table 6 Details of the 3-story, 1-bay buildings under 3D seismic loading

Name	Type	Number of the story in which the vibrating machine is installed
3S1BH1	Modified	1
3S1BH2	Modified	2
3S1BH3	Modified	3
3S1BC1	Conventional	1
3S1BC2	Conventional	2
3S1BC3	Conventional	3

5.2. Isolation of Interior Vibrations

For all the three cases of machinery installments in the modified and the conventional types, the multistory buildings are subjected to horizontal and vertical cyclic vibrations that mimic machine vibrations. These cyclic displacement-controlled loadings are applied at the top of the floating slab in case of modified building. Whereas the loadings are applied on the structural slabs in the conventional buildings to imitate the motion of a rotary machine. Time-displacement histories of the horizontal and vertical vibrations are showcased in Fig. 45 and Fig. 46. These protocols are designed with reference to ACI T1.1-01 (2001) to mimic the vibration of a generating machine.

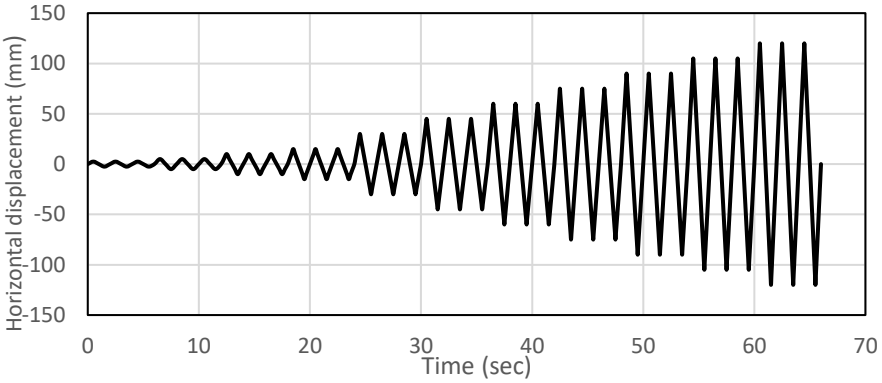

Fig. 45 Horizontal cyclic protocol for the 3-story 1-bay building

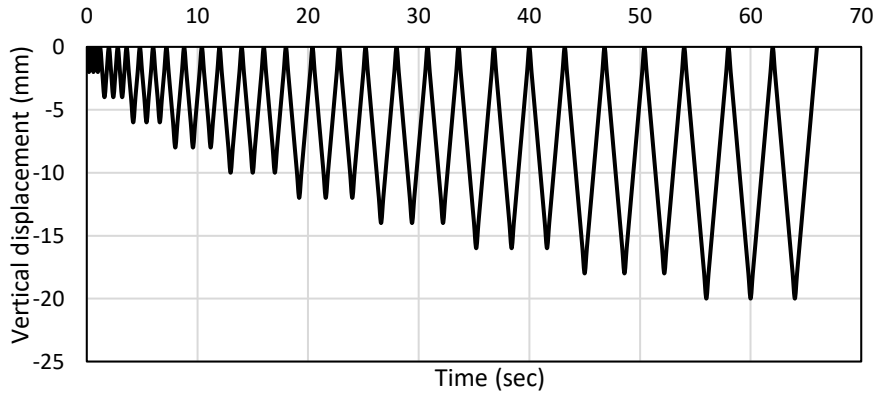

Fig. 46 Vertical half-cyclic protocol for the 3-story 1-bay building

5.2.1. Lateral Drift

a. Story Drift

The vibrating machine is installed in the first, second and third stories. The horizontal loading, which represents the lateral vibration of generating machine, is applied on the floating slab of the modified building and on the structural slab of the conventional buildings.

The resulted lateral drift of each story are depicted in Fig. 47. The new system managed to reduce the lateral drift of each story of the modified building, compared to the conventional building.

Notably, the rate of drift reduction of the three stories is the highest for buildings with FRCISS in the first story. The higher the level, in which the vibrating machine is installed, the less decrement occurs on the sway of the building. Moreover, for vibrating machine installed in a specific story, the drift decreases in less rate for higher levels.

For case 1, lateral drift in 1st, 2nd, and 3rd stories of 3S1BH1 drops by 90.7%, 86.63% and 84.68%, respectively, compared to 3S1BC1. In second case, where the machine is in the 2nd story, the lateral drift reduction in 3S1BH2 is 65.75%, 61.68% and 59.19% compared to the lateral drifts of structural floors 1,2 and 3 of 3S1BC2. The rubber bearings in 3S1BH3 was able to make 53.1%, 45.81% and 42.32% degradation in first, second and third story drifts of 3S1BC3. Fig. 48 shows the six different buildings under the lateral drift. Notably, the drift reduction is higher in lower stories, this may be a result of the higher mass carried by the lower story floor in comparison to the lower mass on the top floor.

b. Inter-story Drift

The inter-story drift, Δ (the difference in horizontal displacement between two consecutive stories divided by the height of the story) is calculated for the three stories. $\Delta_{1\text{-}2}$ and $\Delta_{2\text{-}3}$ are calculated for the difference in maximum drift between first and second stories and second and third stories, respectively.

The inter-story drift in the modified building is compared to the conventional building. Fig. 49 demonstrates the inter-story drift values of the different types of the 3-story 1-bay building. Apparently, the drift ratio – the inter-story drift to the story height – reduces drastically for the adjusted building compared to the conventional building. $\Delta_{1\text{-}2}$ and $\Delta_{2\text{-}3}$ at maximum lateral drift in 3S1BH1 drop by 75.93% and 75.66%, respectively compared to 3S1BC1. In 3S1BH2 they degrade by 58.07% and 53% with respect to 3S1BC2. Likewise, in 3S1BH3, they decrease by 40.77% and 36.84%, respectively in comparison with inter-story drifts in 3S1BC3. It seems that the drift ratio is also decreasing in contrast to the machine elevation. This could be resulted from the mass distribution difference on the different stories, being the highest on the lowest story floor, which enables the floating system to control the lateral drift more effectively.

Furthermore, the drift ratio between the 2nd and 1st stories which represents the column rotation of the 1st story appears to be larger than the column rotation of the 2nd story. This is seen in the multistory buildings with vibrating machines installed in the first and second stories. However, for the case where the machinery is installed in the 3rd story, column rotation of 2nd story is larger compared to 1st story column rotation. It is perhaps caused by third story being unrestricted from the top unlike first and second stories.

According to ACI 318, lateral inter-story drift limit for slab-column connections without shear reinforcement can be taken as 0.5% (Hueste, 2009). Thus, by looking at the drift ratios of hybrid structures, the building with FRCISS installed in the first story has shown a better performance compared to the other two buildings with floating isolation system installed in second and third stories.

Both drift ratios of 2nd and 3rd stories stayed within the drift limit up to 105 mm horizontal displacement (175% shear strain of bearings) for 3S1BH1. Whereas, the inter-story drifts of the mentioned stories exceeded the 0.5% drift ratio at 60 mm displacement (100% shear strain) for 3S1BH2 and 45 mm (75% shear strain) for 3S1BH3, respectively. This also might be due to the larger mass carried by first story slab compared to the second and third stories which results in higher stiffness in the main slab layer for resisting lateral drifts applied on the lifted slab in the specific story that are dissipated largely due to the low stiffness provided by rubber bearings.

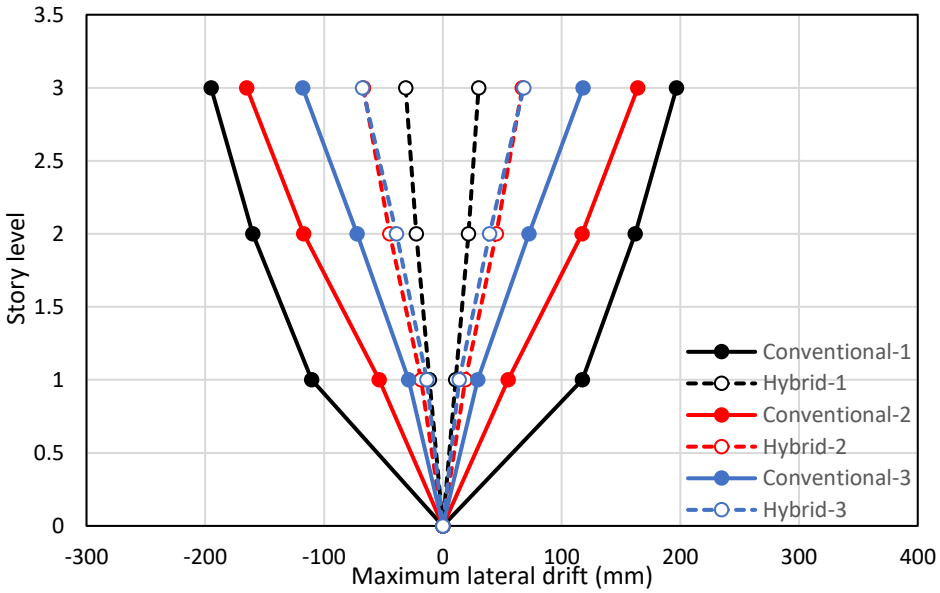

Fig. 47 Maximum positive and negative lateral drifts of 1st, 2nd and 3rd stories of the modified and conventional 3-story 1-bay buildings under horizontal cyclic loading

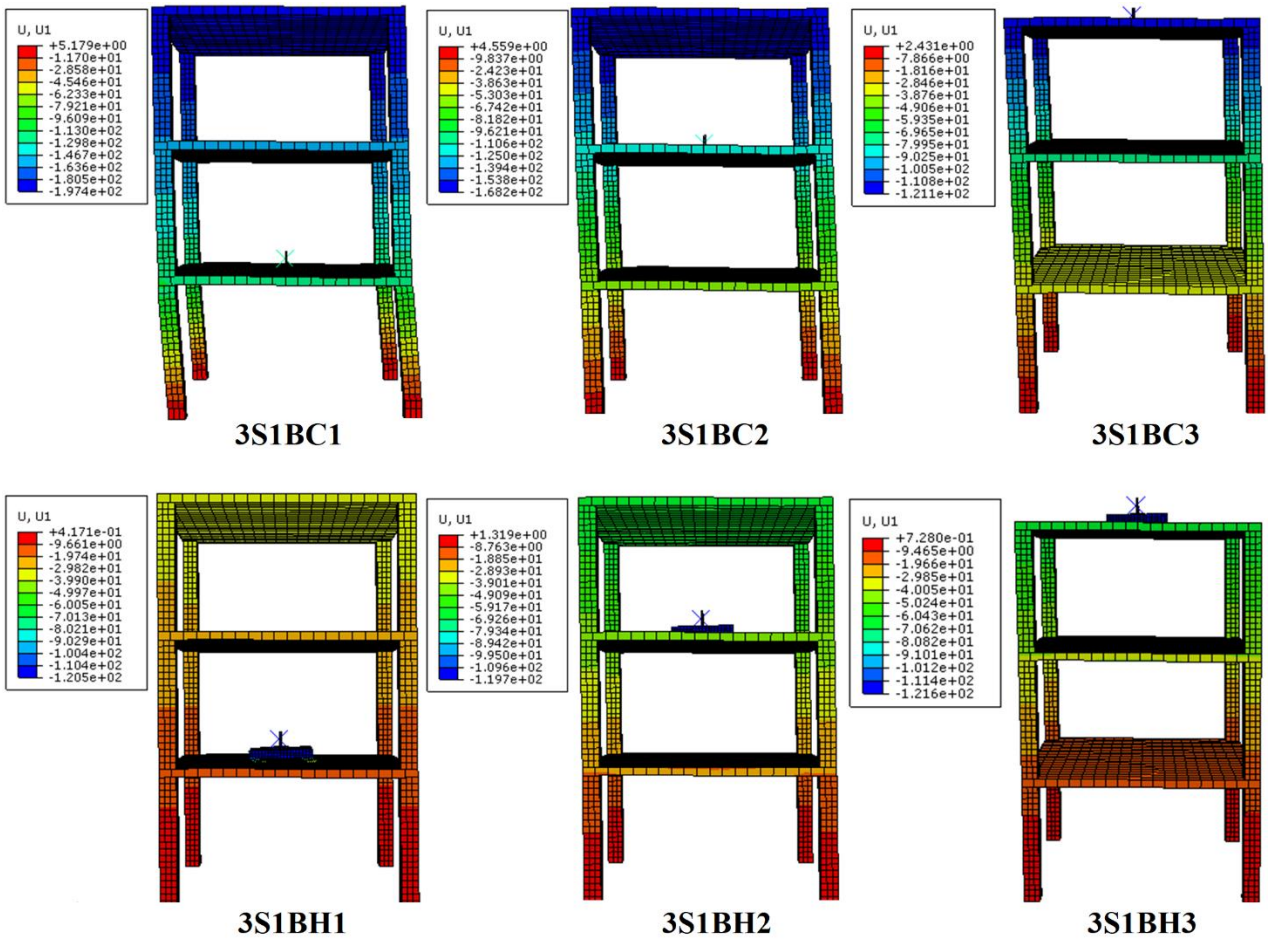

Fig. 48 Lateral deformation of 3-story 1-bay structure with cyclic horizontal loading application with and without FRCISS

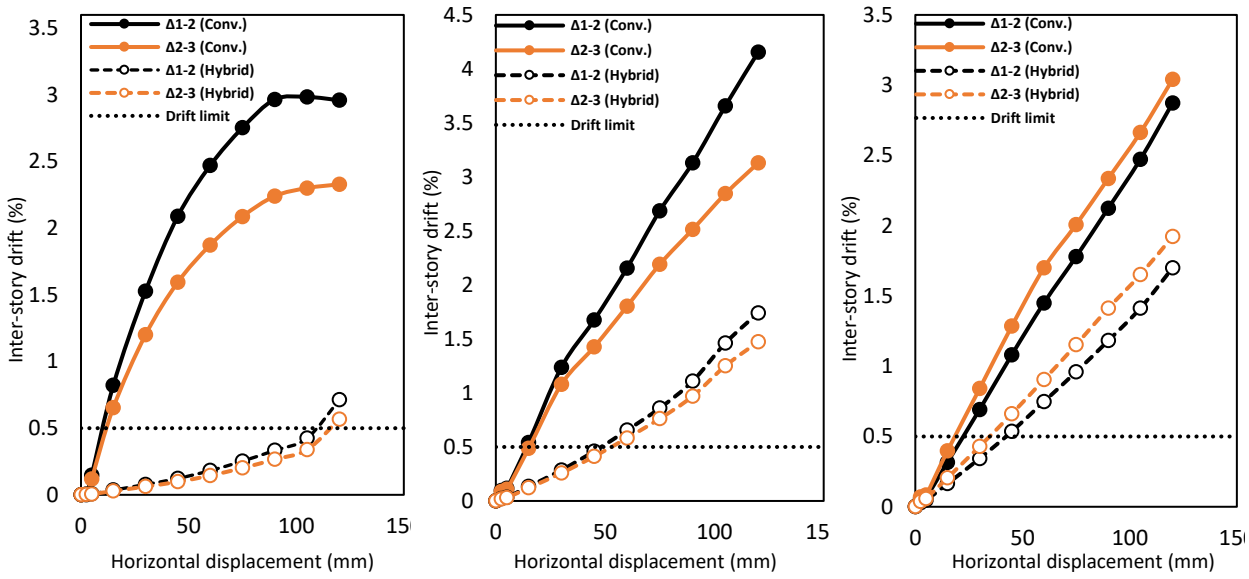

(a) FRCISS in first story (b) FRCISS in second story (c) FRCISS in third story

Fig. 49 Inter-story drift, Δ under horizontal cyclic displacement-controlled loading, applied on conventional and FRCISS slabs of 3-story 1-bay building

Moreover, it's worth noting that for conventional structures, the story drift ratios were beyond drift limit in the first cycle of the loading protocol for 3S1BC1 and 3S1BC2, while 3S1BC3 stayed within the allowable limit in first cycle and crossed it after the 15 mm displacement only.

5.2.2. Deflection

By looking at Fig. 50, it can be seen that the deflection in the stories where the vibrating machine is installed is not affected by the height of the story. The deflection values are the same for all the three cases. This might be a result of the similar constraint cases of the 3 story levels under the vertical loading, which shows that the building mass only affects the horizontal performance. However, deflection of the structural slabs in the modified buildings is clearly reduced when compared to the conventional buildings without FRCISS.

Fig. 51 illustrates the midpoint deflection of the structural slab for the modified and conventional structures with respect to time, taking in consideration that this behavior is the same for all the cases. The HDR bearings and the floating slabs in the adjusted buildings made a 11.1% reduction in the midpoint deflection of the structural slabs in comparison to the maximum deflection in the conventional buildings.

According to ACI 318-14, the deflection limit should not exceed L/240 for RC slabs; L being the structural slab span which equals to 3000 mm for the 3-story 1-bay building. Hence, the deflection limit will be 12.5 mm. As it can be seen from Fig. 51, the deflection in the structural slab of the equipped building has not exceeded the acceptable limit up to 16 mm vertical displacement which corresponded to 26.67% compressive strain in the rubber bearings. Whereas, the structural slab of the conventional building exceeded the allowable deflection earlier, under 14

mm vertical displacement. This indicates the capability of HDR to maintain the deflection in the main slab of the building within the minimum allowable deflection.

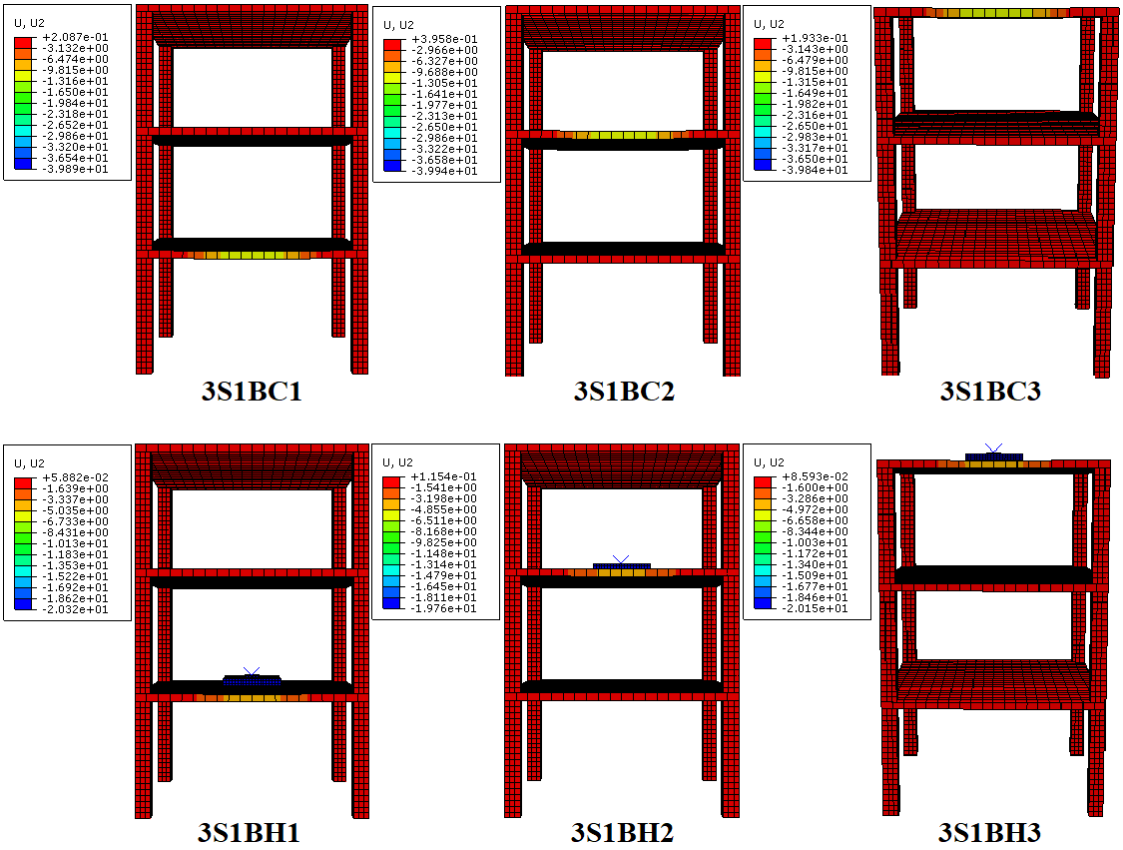

Fig. 50 Deflection of structural slabs in the modified and conventional buildings with the three machinery cases under vertical half-cyclic loading

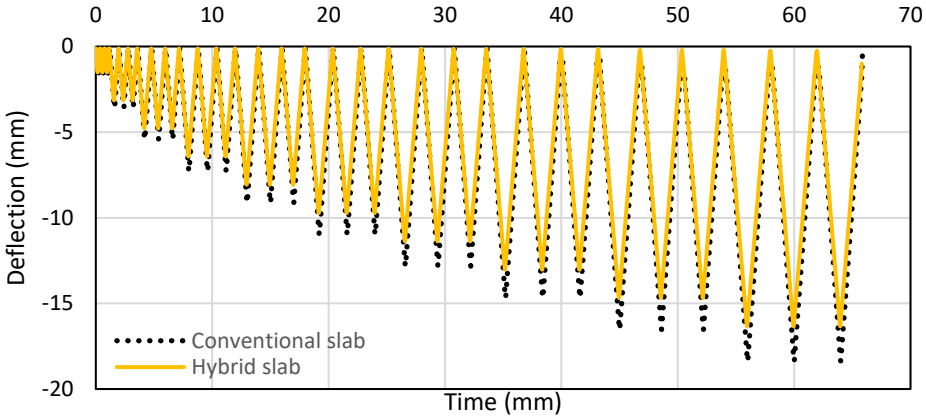

Fig. 51 Midpoint deflection of the structural slabs of modified and conventional buildings

5.2.3. Frequency Analysis

Generally, machines generate different frequencies ranging between 1 Hz and 60 Hz. By assuming that a vibrating machine installed in the first story of the building, a sinusoidal movement

has been applied to the floating slab of the building structure with 30mm amplitude. In order to evaluate effect of frequency on response of structure, the various frequencies have been considered for the applied movement in range of 5 Hz to 60 Hz include of 1Hz, 5Hz, 10Hz, 30Hz, 60Hz.

By conducting the free vibration analysis, the natural frequency for the 3-story 1-bay structure is determined as 1.82 Hz. Since the floating slab system is installed on the rigid bottom slabs, therefore, the natural frequency of the frame with floating slab also remains the same. Hence the same frequency of the frame (1.82Hz) also is considered for excitation of machine to evaluate response of structure when the frequency of applied movement is same as natural frequency of structure.

The FE results for response of structure in terms of the displacement of tip node of frame versus time are presented in Fig. 52 for various frequencies of excitation. Also effect of various applied excitation frequencies on response frequency has been demonstrated in Table 7.

The results are showing the drastic reduction in building's response amplitude with respect to the applied amplitude on the floating slab. However, if frequency ratio (β) is defined as:

$$\beta = \frac{Frequency\ of\ excitation}{Frequency\ of\ Structure} \qquad (1)$$

For excitation with 1 Hz which led to β less than 1, the amplitude reduction is around 75%, however by increase of β more than 1 in frequencies of 5Hz, 10Hz, 30Hz and 60Hz, this reduction is noticeable increased in range of 86% to 92%. Hence the minimum amplitude reduction is happened in β equal to 1, when the frequency of vibration machine is same to natural frequency of structure as 1.82Hz and the resonance occurred. Although high structural oscillations expected when resonance happened, however function of high damping rubber in absorbing machine vibration is lead to dissipate structural movements in all renege of excitation frequencies even when the β is 1. It is proving efficiency of proposed floating slab with HDR bearing to diminish effect of applied excitations on structural response.

As it can be seen in the results, the response frequency of the structure is also affected by the presence of the floating system, and it resulted to lower response frequency in comparison to the frequency of applied excitation. This deduction is increased in higher excitation frequency, whereas in 1Hz excitation, 21% deduction has been perceived in response frequency, but in 60Hz excitation frequency, the reduction has been risen to 42% (Table 7).

Table 7: Response of frame under applied excitation with various frequencies

Structure response	**Frequency**					
	1 Hz	1.82 Hz	5 Hz	10 Hz	30 Hz	60 Hz
Displacement of tip node (mm)	7.28	12.42	3.9	3.12	2.82	2.37
Displacement reduction (%)	75.7%	58.6%	86.8%	89.8%	90.6%	92.1%
Frequency of Response	0.79 Hz	1.7 Hz	3.08 Hz	5.95 Hz	17.49 Hz	34.52 Hz
Frequency difference (%)	21%	6.6%	38.4%	40.5%	41.7%	42.47%

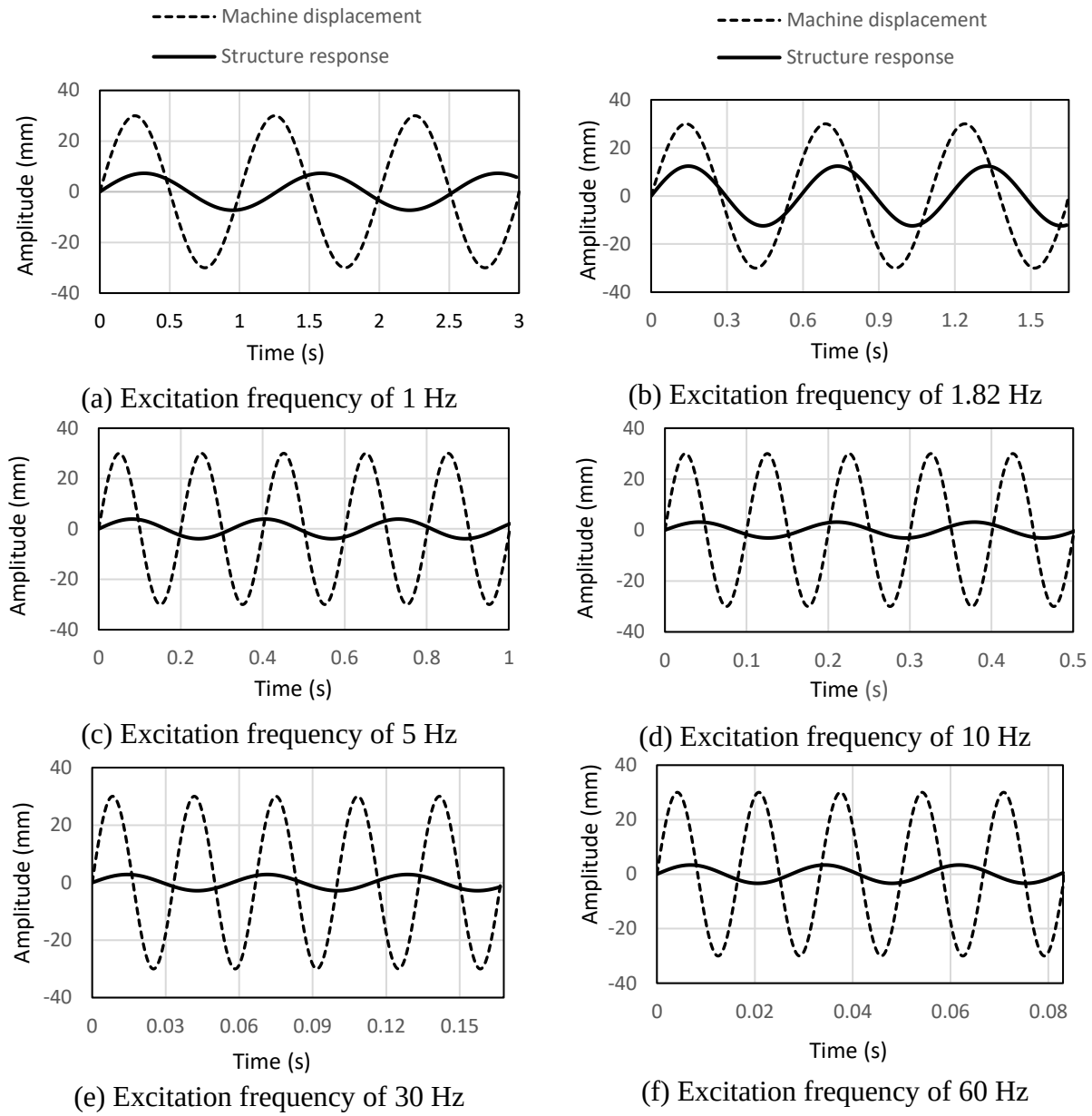

(a) Excitation frequency of 1 Hz

(b) Excitation frequency of 1.82 Hz

(c) Excitation frequency of 5 Hz

(d) Excitation frequency of 10 Hz

(e) Excitation frequency of 30 Hz

(f) Excitation frequency of 60 Hz

Fig. 52 Machine displacement and structure response vs. time for various machine excitation frequencies

5.3. Isolation of Exterior Vibrations

The floating rubber-concrete slab system has proven to be an efficient tool in isolating horizontal and vertical vibrations, induced on the floating slab, from transmitting to the rest of the building by dissipating the energy along the rubber height. However, structural elements of the multi-story buildings are not exposed to interior machinery vibrations only. They are also vulnerable to exterior vibrations that can cause damage to the structural elements and machinery as well. Seismic vibration is an example of such source of damage.

The capability of the rubber system in dealing with these vibrations is examined by conducting an acceleration time-history analysis. Three components of El Centro (1940); N_S; E_W; and up

and down time histories of 10 seconds durations each (Fig. 53), have been applied at the base level of the 3-story 1-bay building of the recent study. The geometry and the details of the 3-story 1-bay buildings are previously discussed and shown in Fig. 44 and Table 6, respectively.

The resulting 3D deformations are studied and analyzed by comparing the modified building with the conventional building under the same seismic components. The time-displacement data are extracted from a midpoint of the structural slabs in conventional building and the structural and floating slabs in modified buildings. A 5-ton, which is assumed for the machinery mass, is applied on the slab in which the vibrating machine is installed and the whole buildings are subjected to gravity loads.

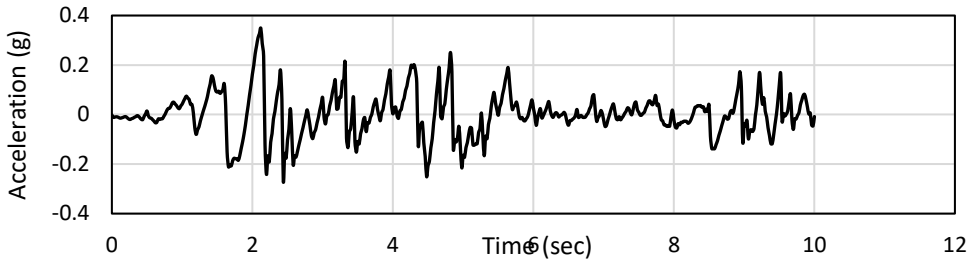

(a) North-South component

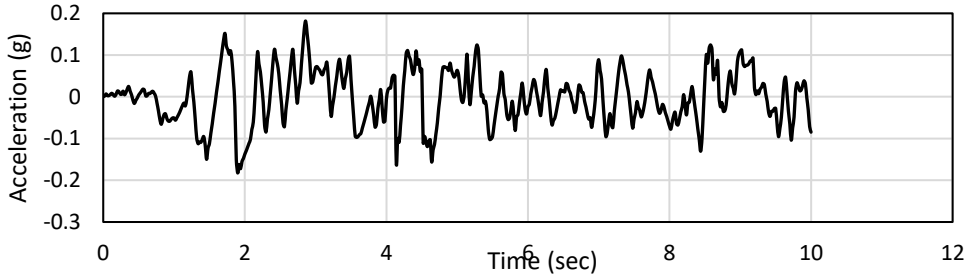

(b) East-West component

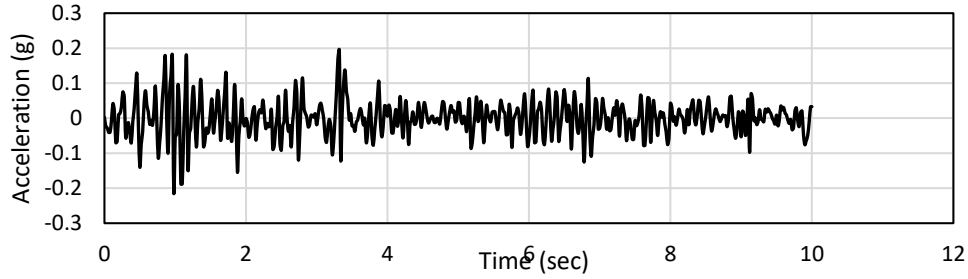

(c) Up-Down component

Fig. 53 The three components of El Centro 1940 earthquake with 10 seconds duration

The hysteretic behavior of the considered 3 storey frame when subjected to the three components of El-Centro earthquake is plotted in Fig. 53, which illustrates the force-displacement response of the structure during applied seismic excitation. The ultimate bearing capacity in each of the three directions is shown in these graphs which reached to approximate peak forces for the two lateral components of N-S and E-W as 82.56 KN and 86.17 KN respectively, while for the vertical direction (up-down), 122.7 KN force is obtained. This is due to the higher stiffness of the structure in the vertical direction in addition to effect of structure weight.

During earthquake excitation, the rubber bearings under floating slabs dissipate the movement transferring between the floating slab and frame and diminish vibration effect.

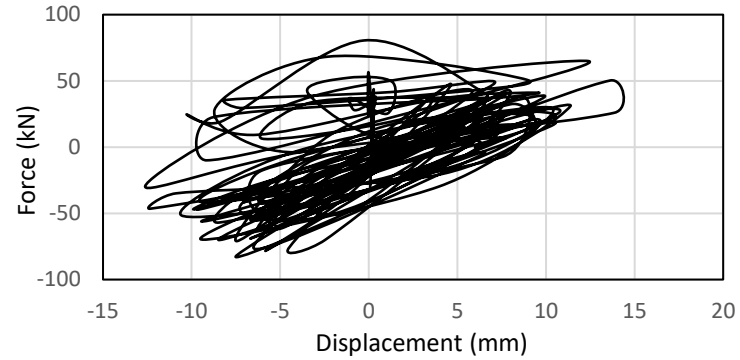

(a) North-South component

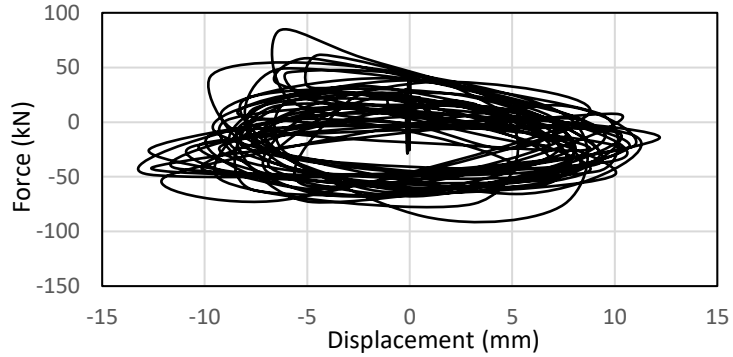

(b) East-West component

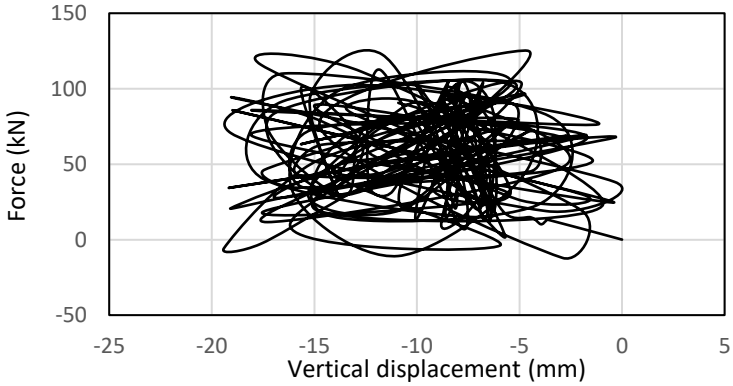

(c) Up-Down component

Fig. 54 Force-displacement hysteresis results of structure under applied 3D seismic excitation

5.3.1. Lateral Seismic Components

Two of the three components of El Centro earthquake strike the building horizontally; N_S and E_W components, which act in the orthogonal x and z directions, respectively. From the data collected for the building with the floating system, it's clear that the difference in lateral drifts of the structural and floating slabs in each case depend on the level of the floor where the vibrating machine is installed. The comparison between the two types of buildings is based on the difference in area under the curve between the time-displacement of the modified and conventional curves.

In the first case for the modified building 3S1BH1, where the vibrating machine is installed in the first story, the rubber bearings caused the maximum lateral drift under the N_S component in the x-direction for the 1st, the 2nd, and the 3rd stories to be less than the conventional building 3S1BC1 by 70.37%, 69.18% and 69.48%, respectively. The maximum displacement of the floating

slab was 14.06% less than the structural slab beneath which indicates that the bearings managed to dissipate vibrations on the floating slab and the machine as well (Fig. 55 a). Likewise, the lateral orthogonal drifts under the E_W component in the z-direction performed almost similarly for the both types of buildings (Fig. 55 b). The HDR bearings installed under the vibrating machine have caused a decrement in the maximum lateral drifts of the first, second and third stories from the conventional floors drifts by 74.86%, 73.68% and 73.54%, respectively. The floating slab has drifted 15.02% less than the structural slab below it in the z-direction due to the presence of HDR in between.

For 3S1BH2, the peak lateral drift of the three stories under the N_S component of El Centro earthquake have minimized by 27.19%, 25.7% and 25.35% with respect to 3S1BC2 for 1st, 2nd and 3rd stories, respectively. Whereas, the rubber bearings caused an 11.8% reduction in the upper slab compared to the lower slab of the 2nd story (Fig. 55 c). Similarly, under the E_W component, 18.55%, 16.7% and 16.03% displacement reduction have occurred in the modified building in comparison to the conventional building. The upper slab has decreased in terms of lateral drift by 10.88% from the structural slab beneath (Fig. 55 d).

Finally, for 3S1BH3, the lateral drifts of the 1st, the 2nd and the 3rd stories under the north south components got lowered by 21.5%, 19.92% and 19.12%, respectively, compared to the conventional building 3S1BC3. The floating slab was 10.97% less than the structural slab of the 3rd story of 3S1BH3 (Fig. 55 e). For the E_W component on the same building, the drifts of the stories of the levels; 1, 2 and 3 have dropped by 18.13%, 16.29% and 15.24%, respectively from the building with no rubber bearings. The lateral displacement of the upper slab of the third story has stepped back by 9.46% from the respective floor slab (Fig. 55 f).

It's clear that the installment of the vibrating machine on a floating slab foundation with HDR bearings between the upper and the lower structural slab can influence the behavior of the multi-story building under a seismic hazard. The lateral drift data comparison shows an improvement in the reaction of the overall structure when using rubber pads to isolate the machinery. The adjusted system in this case functions similarly to a tuned mass damper (TMD) by dissipating the displacement of the high-rising building. It also works as a passive isolation under the vibrating machine; damping the vibrations generated on the machine during the earthquake by dissipated the energy along the rubber bearings. It's noted that the higher the level of vibrating machine installment, the more the 3-story, 1-bay building drifts laterally under the north south and east west components of El Centro.

5.3.2. Vertical Seismic Component

Apart from the horizontal components of El Centro earthquake, the vertical component affects the 3-story, 1-bay building distinctly. In all the three cases where the vibrating machine is installed in the first, second and third stories, respectively, the vertical displacements taken at the midpoint of each slab of the building perform almost similarly (Fig. 56 a, b and c).

For the building where the machines are attached at the first and second stories, the vertical displacements of the story slabs where no machines are installed range between 0 and 20 mm downwards. However, the frequency of the vibration is doubled and more symmetric for the buildings with floating systems. In the stories of 3S1BC1, 3S1BC2 and 3S1BC3 where the machines are installed, the structural slabs deflected frequently between (34.1 – 65.1) mm, (31.9 – 65.8) mm and (39.4 – 72.3) mm downwards, respectively with the latter displacing around further deflected point than the first two cases.

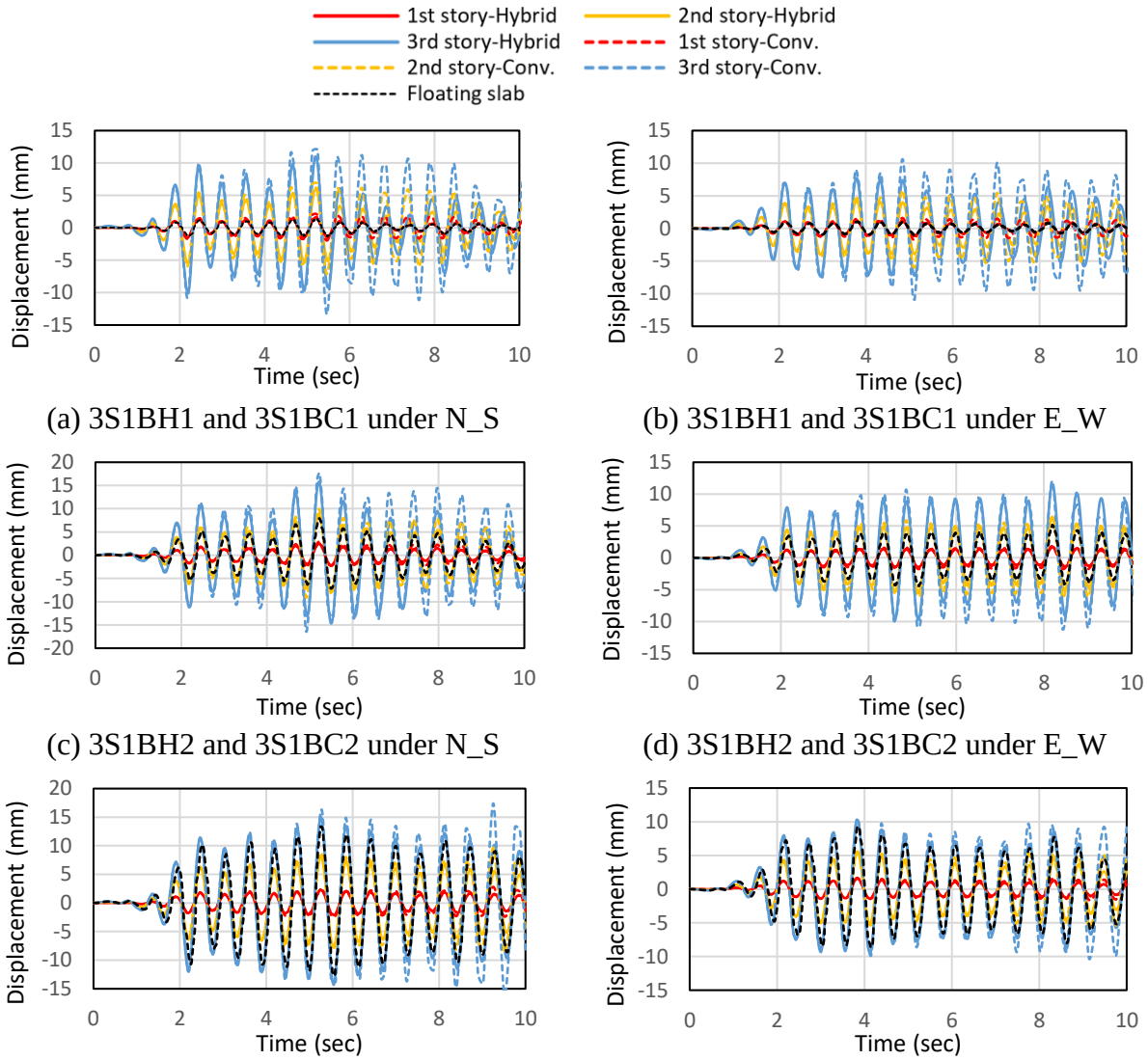

(a) 3S1BH1 and 3S1BC1 under N_S

(b) 3S1BH1 and 3S1BC1 under E_W

(c) 3S1BH2 and 3S1BC2 under N_S

(d) 3S1BH2 and 3S1BC2 under E_W

(e) 3S1BH3 and 3S1BC3 under N_S

(f) 3S1BH3 and 3S1BC3 under E_W

Fig. 55 Comparison between the deformation of the modified and the conventional building under N_S and E_W seismic components

By applying the floating systems to the buildings, the deflection of the structural slabs under the effect of the vertical component of the seismic hazard changed drastically. Despite the presence of the rubber bearings, it was noted that the structural slabs of 3S1BH1, 3S1BH2 and 3S1BH3 displaced in a lower point compared to the counter apart conventional buildings. However, the vertical vibration was damped gradually unlike the conventional case where the vibration amplitude was almost the same during the earthquake. It's worth noting that the structural slab in both 3S1BH3 and 3S1BC3 deflected further compared to the first two cases. This may be a result of the structural slab being supported by columns on the lower side only when compared to the other two cases where the structural slabs in the first and second stories are supported on both upper and lower faces by columns. The HDR pads have also produced a suitable damping rate to the floating slabs under the vibrating machines with respect to the structural slabs beneath. The vertical displacement has dropped in the upper floating slabs of 3S1BH1, 3S1BH2 and 3S1BH3 compared to the structural slabs of the same stories by 11.45%, 11.21% and 10.95%, respectively.

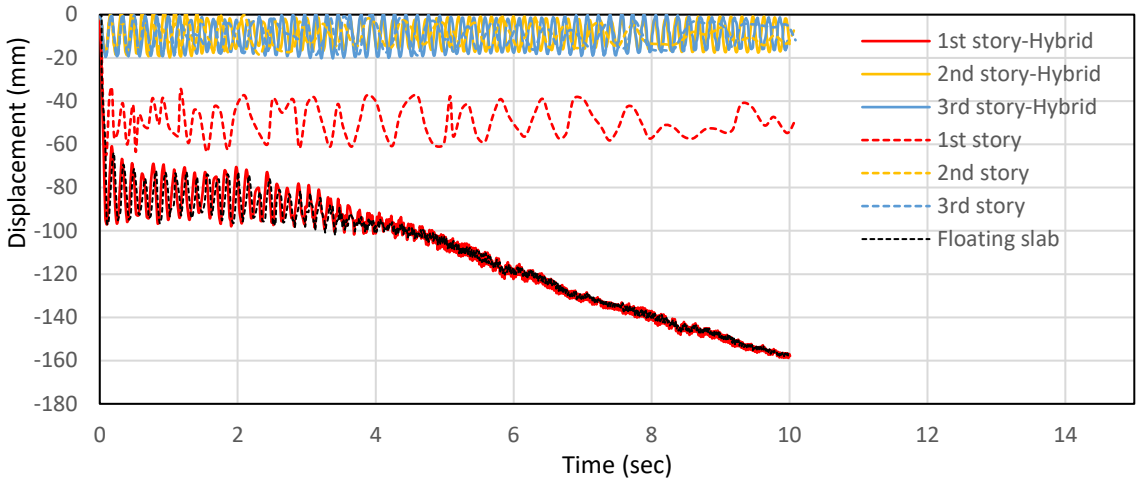

(a) 3S1BH1 and 3S1BC1

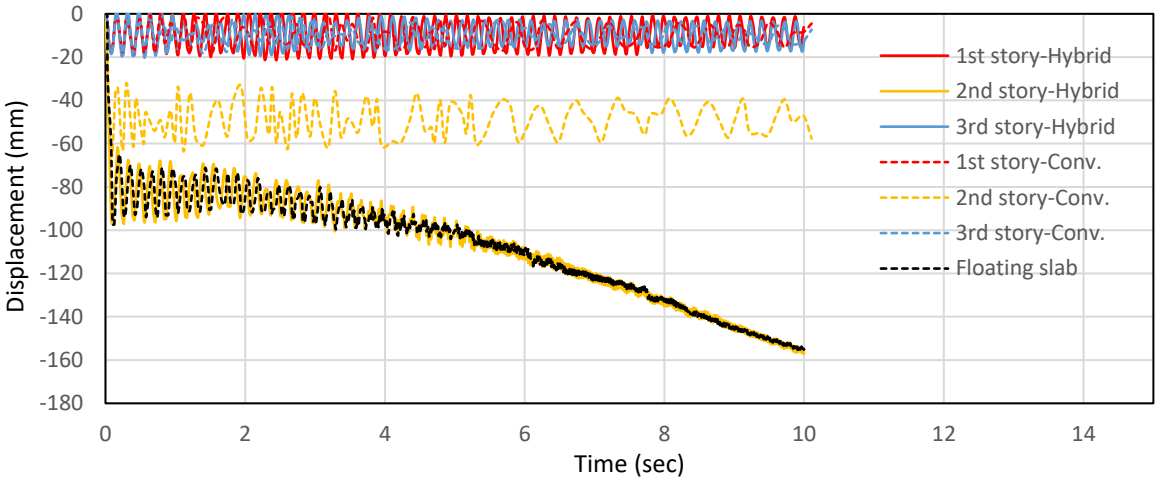

(b) 3S1BH2 and 3S1BC2

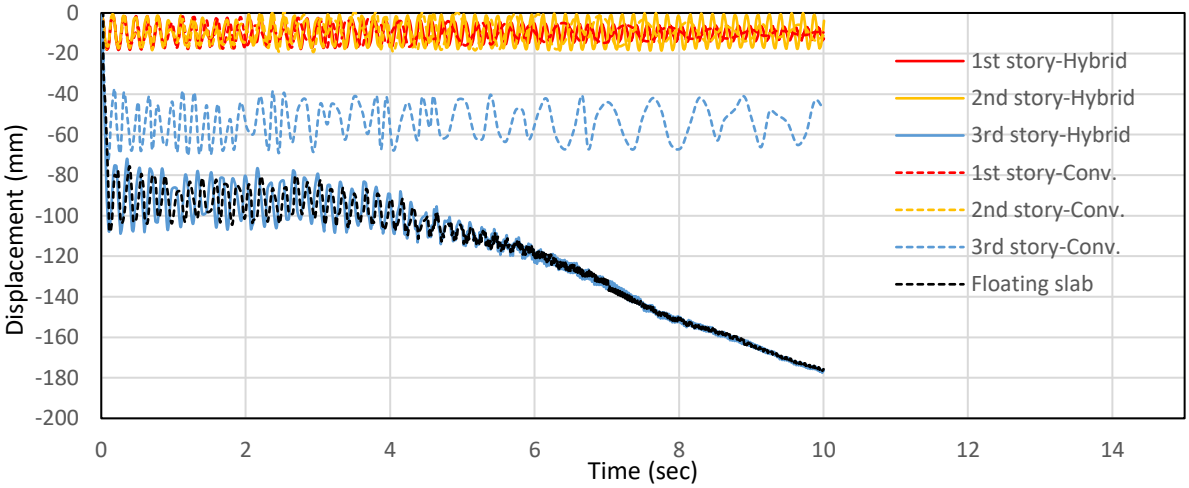

(c) 3S1BH3 and 3S1BC3

Fig. 56 Comparison between the deformation of the modified and the conventional building under Up and Down component

6. Conclusions

In this study, a floating rubber-concrete isolation slab system (FRCISS) is developed by implementing high damping rubber (HDR) as the isolation material to use in structures subjected to horizontal and vertical vibrations due to machinery or other source of loads.

For this purpose, the numerical simulations have been conducted and two prototypes of FRCISS slabs have been casted and experimentally tested by applying cyclic load which the main findings of this research study are summarized as:

- HDR bearings are able to mitigate 3D machine vibrations induced on the floating slab and transmitting to the structural slab beneath. Shear stiffness in specimen HC has decreased by 70.2% of the initial shear stiffness and the damping ratio reached 14.8%. Whereas, compressive stiffness in specimen VC stayed constant about 0.9 KN/mm with marginal damping. However, the deflection in the structural slab was reduced by 29.25% with respect to the vertical displacement of the floating slab (upper slab).
- Experimental testing showed the possibility of FEM in predicting the behavior of the proposed FRCISS under horizontal and vertical vibrations.
- HDR bearings are capable of damping interior vibrations in multistory buildings. The application of the FRCISS in a 3-story, 1-bay building in different story levels, where the machinery is installed, is efficient in controlling both lateral drifts and deflections of the structural slabs. The lower the level of the vibrating machine gets, the less drifted the stories, compared to the conventional 3-story 1-bay building where vibrating machine is installed directly to the structural slab of the respective level. The lateral drifts in the structures with floating systems in the 1st, 2nd, and 3rd stories under horizontal cyclic loading were reduced by an average 87.33%, 62.21% and 47.08%, compared to lateral drifts in conventional structures, respectively. However, the deflection reduction is not influenced by the elevation of the machine-equipped story, it reduced by 11.1%.
- HDR can deal with exterior vibrations as the rubber-floating slab functions as a tuned mass damper (TMD). Seismic analysis on the 3-story 1-bay building under 3D components of El Centro 1940 earthquake showed the huge effectiveness of high damping rubber in minimizing deformations under seismic hazards. Similar to the effect of HDR on interior vibrations, the lateral deformations in the 3-story building under seismic forces are smaller for lower story levels and the vertical deformations in the structural slabs are almost identical for the different machinery elevations. the average drift reduction values were 69.68%, 26.08%, and 20.18% under the north-south seismic component, and 74.03%, 17.1%, and 16.55% under the east-west seismic component, for the modified buildings compared to conventional buildings.
- The FRCISS is also capable of protecting the vibrating machine from earthquakes by reducing the 3D deformations on the floating slabs where the rotary machines are installed.

References

ACI 318 (2014), Building code requirements for structural concrete and commentary, American Concrete Institute; Farmington Hills, MI, USA.

Ahmadi, H. and Fuller, K. (2004), “Goodchild I. Novel devices for the isolation of floors against earthquakes and ambient vibrations”, *The 13th World Conference on Earthquake Engineering*, Vancouver, B.C., Canada, Paper No. 2216.

Almeida, AFO., Inácio, MMG., Lúcio, VJG., and Ramos, AP., (2016), “Punching behaviour of RC flat slabs under reversed horizontal cyclic loading”, *Engineering Structures*, **117**, 204–219.

Al-Rifaie, H., Glema, A., and Malendowski, M., (2015), "Vertical seismic load effects on the response of structures with toggle brace dampers", *Proceedings of the Fifteenth International Conference on Civil, Structural and Environmental Engineering Computing*, Prague, Czech Republic, 1–19.

Anajafi, Hamidreza, and Medina RA. (2018), "Comparison of the seismic performance of a partial mass isolation technique with conventional TMD and base-isolation systems under broad-band and narrow-band excitations". *Engineering Structures 158*, 110–123.

Bergamo, E., Fasan, M., and Bedon, C. (2020), "Efficiency of coupled experimental-numerical predictive analyses for inter-story floors under non-isolated machine-induced vibrations", *Actuators*, **9**(3), 87, Multidisciplinary Digital Publishing Institute.

Button, MR., Cronin, CJ., and Mayes, RL. (2002), "Effect of vertical motions on seismic response of highway bridges", *Journal of Structural Engineering*, **128** (12), 1551–1564.

Casagrande, L., Villa, E., Nespoli, A., Occhiuzzi, A., Bonati, A., and Auricchio, F. (2019), "Innovative dampers as floor isolation systems for seismically-retrofit multi-storey critical facilities", *Engineering Structures 201*, 109772, 1–14.

Castellano, MG., Dusi, A., and Poggianti, A. (2015), "Testing of high damping rubber bearings and lead rubber bearings for nuclear power plants", S*ECED 2015 Conference: Earthquake Risk and Engineering towards a Resilient World*, Cambridge UK, 1–10.

Chen, Z., Popovski, M., and Ni, C. (2020), "A novel floor-isolated re-centering system for prefabricated modular mass timber construction – Concept development and preliminary evaluation", *Engineering Structures 222*, 111168.

Cu, VH., Han, B., and Pham, DH. (2017), "Tuned mass-high damping rubber damper on a taut cable", *KSCE Journal of Civil Engineering*, **21** (3), 928–936.

Elnashai, AS. and Papazoglou, AJ. (1997), "Procedure and spectra for analysis of RC structures subjected to strong vertical earthquakes loads", *Journal of Earthquake Engineering*, **1** (1), 121–155.

Foglar, M. and Göringer, J. (2015), "Influence of cyclic loading on the deflection development of concrete specimens", *The Civil Engineering Journal*, **4**, 1–22.

Gowardhan, SD. and Deosarkar, MU. (2015), "Protection of the buildings from the earthquake risk using high damping rubber bearing", J*ournal of Civil Engineering and Environmental Technology*, **2** (12), 27–31.

He, C., Zhou, S., and Guo, P. (2020), "An efficient three-dimensional method for the prediction of building vibrations from underground railway networks", *Soil Dynamics and Earthquake Engineering 139*, 106269, 1–15.

Hu, X. and Zhou, Z. (2020), "Seismic analysis of a reinforced concrete building isolated by high damping rubber bearings using deformation history integral type model", *The Structural Design of Tall and Special Buildings*, **29** (18), 1–13.

Hueste, M., Kang, T., and Robertosn, I. (2009), "Lateral drift limits for structural concrete slab-column connections including shear reinforcement effects", *Proceedings of the 2009 Structures Congress – Don't Mess with Structural Engineerings: Expanding Our Role*, 1–10.

Hui, CK. and Ng, CF. (2009), "Attenuation of flexural vibration for floating floor and floating box induced by ground vibration", *Applied Acoustics*, **70**, 799–812.

Hui, CK. and Ng, CF. (2007), "New floating floor design with optimum isolator location", *Journal of Sound and Vibration*, **193** (1), 175–184.

Jin, H., Zhou, S., and Liu, W. (2015), "An experiment to assess vibration reduction ability of the rubber floating-slab tracks with different supporting forms", *Journal of Vibroengineering*, **17** (6), 3237–3246.

Karabork and Turan (2011), "Performance of multi-storey structures with high damping rubber bearing base isolation systems", *Structural Engineering and Mechanics*, **39** (3), 399–410.

Kim, TM., Kim, JT., and Kim, JS. (2018), "Effect of structural vibration and room acoustic modes on low frequency impact noise in apartment house with floating floor", *Applied Acoustics*, **142**, 59–69.

Liang, L., Li, X., Yin, J., Wang, D., Gao, W., and Guo, Z. (2019), "Vibration characteristics of damping pad floating slab on the long-span steel truss cable-stayed bridge in urban rail transit", *Engineering Structures 191*, 92–103.

Mukherjee, S. (2017), "A theoretical study and 3d modeling of nonlinear passive vibration isolator", *International Journal of Applied and Advanced Scientific Research*, **2** (2), 159–168.

Naeim, F. and Kelly, JM. (1999), "Design of seismic isolated structures: from theory to practice", *New York: John Wiley & Sons*.

Okwudire, CE. and Lee, J. (2013), "Minimization of the residual vibrations of ultra-precision manufacturing machines via optimal placement of vibration isolators", *Precision Engineering*, **37** (2), 425–432.

Pan, P., Shen, S., Shen, Z., and Gong, R. (2018), "Experimental investigation on the effectiveness of laminated rubber bearings to isolate metro generated vibrations", *Measurements*, **122**: 554–562.

Quaglini, V., Dubini, P., and Vazzana, G. (2016), "Experimental assessment of high damping rubber under combined compression and shear", *Journal of Engineering Materials and Technology*, **138**, 1–9.

Ramkrisna, S., Darji, V., and Purohit, SP. (2006), "Design of base isolator for r.c.c. building & performance evaluation", Conference Paper.

Rha, C., Kang, TH-K., Shin, M., and Yoon, JB. (2014), "Gravity and lateral load-carrying capacities of reinforced concrete flat plate systems", *ACI Structural Journal*, **111** (4), 753–764.

Robertson, IN. and Johnson, GP. (2004), "Non-ductile slab-column connections subjected to cyclic lateral loading", *13th World Conference on Earthquake Engineering*, Vancouver, B.C., Canada, Paper No. 143.

Robertson, IN., Kawai, T., Lee, J., and Enomoto, B. (2002), "Cyclic testing of slab-column connections with shear reinforcement". *ACI Structural Journal*, 605–613.

Sunaryati, J., Adnan, A., and Ramli, MZ. (2008), "Evaluation of the laminated hollow circular elastomeric rubber bearing", *The 14th World Conference on Earthquake Engineering*, Beijing, China.

Warn, GP. and Whittaker, AS. (2008), "Vertical earthquake loads on seismic isolation systems in bridges" *Journal of Structural Engineering*. **134**, 1696–1704.

Wei, W., Tan, P., Yuan, Y., and Zhu, H. (2019), "Experimental and analytical investigation of the influence of compressive load on rate-dependent high-damping rubber bearings", *Construction and Building Materials 200*, 26–35.

Woon, KS. and Hejazi, F. (2019), "Horizontal cyclic performances of hook-end U-shaped high-damping rubber jointed precast frame", *International Journal of Civil Engineering*, 1–16.

Woon, KS. and Hejazi, F. (2019), "Vertical cyclic performance of precast frame with hook-end U-shaped high-damping rubber joint", *KSCE Journal of Civil Engineering*, **23** (5), 2215–2226.

Xiang, Y., Koetaka, Y., and Okuda, N. (2019), "Single-story steel structure with LVEM-isolated floor: Elastic seismic performance and design response spectrum", *Engineering Structures 196*, 109314, 1–17.

Xiang, Y. and Koetaka, Y. (2019), "Structural feasibility of incorporating the LVEM-isolated floor in the first story of a two-story steel frame", *Engineering Structures 199*, 109686, 1–18.

Yoo, B., Lee, JH., and Koo, GH. (1996), "Comparison of analysis results with experimental results for ENEA and CRIEPI rubber bearings", 1996 KAERI, Republic of Korea.